POLITECNICO DI TORINO
Repository ISTITUZIONALE

Two boundary integral equation methods for linear elastodynamics problems on unbounded domains

Original
Two boundary integral equation methods for linear elastodynamics problems on unbounded domains / Falletta, S., Monegato, G., Scuderi, L.. - In: COMPUTERS & MATHEMATICS WITH APPLICATIONS. - ISSN 0898-1221. - STAMPA. - 78:(2019), pp. 3841-3861. [10.1016/j.camwa.2019.06.017]

Availability:
This version is available at: 11583/2735555 since: 2019-11-08T10:42:05Z

Publisher:
Elsevier

Published
DOI:10.1016/j.camwa.2019.06.017

Terms of use:

This article is made available under terms and conditions as specified in the corresponding bibliographic description in the repository

Publisher copyright
Elsevier postprint/Author's Accepted Manuscript

© 2019. This manuscript version is made available under the CC-BY-NC-ND 4.0 license
http://creativecommons.org/licenses/by-nc-nd/4.0/.The final authenticated version is available online at:
http://dx.doi.org/10.1016/j.camwa.2019.06.017

(Article begins on next page)

14 October 2026

Two boundary integral equation methods for linear elastodynamics problems on unbounded domains *

S. Falletta†, G. Monegato‡, L. Scuderi§

Abstract

We consider (transient) 3D elastic wave propagation problems in unbounded isotropic homogeneous media, which can be reduced to corresponding 2D ones. For their solution, we propose and compare two boundary integral equation approaches, both based on the coupling of a discrete time convolution quadrature with a classical space collocation discretization. In the first approach, the PDE problem is preliminary replaced by the equivalent well known (vector) space-time boundary integral equation formulation, while in the second, the same PDE is replaced by a system of two (coupled) wave equations, each one of which is then represented by the associated boundary integral equation. The construction of these two approaches is described and discussed. Some numerical testing are also presented.

KEY WORDS: elastic wave propagation; space-time boundary integral equations; discrete convolution quadrature; collocation method.

1 Introduction

In this paper we consider (transient) 3D elastic wave propagation problems in unbounded isotropic homogeneous media, which can be reduced to corresponding 2D ones. This is the case, for example, of problems defined on the exterior of a bounded rigid domain, which are invariant in one of the cartesian directions.

For their solution, in the next section we first apply a classical space-time boundary integral formulation approach (see, for example, [4, 18]), which is then discretized by combining a discrete time convolution quadrature with a classical space collocation method (see [7, 8]). Approaches of this type, with the collocation discretization replaced by a Galerkin one, have been already used by several authors to solve 3D elastodynamic interior problems (see, for example, [10, 2, 13]); for 2D problems see [17].

*We acknowledge that the present research has been performed in the framework of MIUR grant Dipartimenti di Eccellenza 2018-2022 and supported by GNCS-INDAM 2018 research program: Sviluppo di tecniche efficienti e accurate per metodi BEM.

†Dipartimento di Scienze Matematiche, Dipartimento di Eccellenza 2018-2022, Politecnico di Torino, Italy. Email: silvia.falletta@polito.it

‡Dipartimento di Scienze Matematiche, Dipartimento di Eccellenza 2018-2022, Politecnico di Torino, Italy. Email: giovanni.monegato@polito.it

§Dipartimento di Scienze Matematiche, Dipartimento di Eccellenza 2018-2022, Politecnico di Torino, Italy. Email: letizia.scuderi@polito.it

In Section 3, by applying a classical Helmholtz decomposition, we split the elastic (vector) equation into a couple of scalar wave equations, describing, respectively, the propagation of P-waves and S-waves. The two equations are coupled by the problem Dirichlet boundary conditions. This splitting has been used in [3] to solve an interior problem by a finite element method. Instead, here the two aforesaid scalar equations are reformulated in terms of their associated space-time BIE representations, which are then discretized by the corresponding time convolution quadratures and a space collocation method. This approach, inherently allows to include P- and S-wave sources.

In Section 4 we perform some testing and comparison on the two approaches.

2 The standard BIE formulation for elastodynamics

Because of the assumptions we have made in the introduction, we define by $\Omega^i \subset \mathbb{R}^2$ an open, bounded and rigid domain, whose boundary Γ is assumed to be a closed and smooth (at least C^3-continuous) curve, or the union of a finite number of separated domains of this type. Then, we set $\Omega^e = \mathbb{R}^2 \setminus \overline{\Omega^i}$ and $\overline{\Omega^e} = \mathbb{R}^2 \setminus \Omega^i$.

The linear elastodynamics problem that characterizes small variations of a displacement field $\mathbf{u}(\mathbf{x},t) = (\mathrm{u}_1(\mathbf{x},t), \mathrm{u}_2(\mathbf{x},t))$, $\mathbf{x} = (x_1, x_2)$ in a homogeneous isotropic elastic medium Ω^e, caused by a body force $\mathbf{f}$, initial conditions $\mathbf{u}_0, \mathbf{v}_0$ locally supported and a Dirichlet datum $\mathbf{g}$, is defined by the following system:

$$\begin{cases} \rho\,\dfrac{\partial^2 \mathbf{u}}{\partial t^2}(\mathbf{x},t) - (\lambda+\mu)\nabla(\operatorname{div}\mathbf{u})(\mathbf{x},t) - \mu\,\nabla^2\mathbf{u}(\mathbf{x},t) & = \mathbf{f}(\mathbf{x},t) \quad (\mathbf{x},t) \in \Omega^e \times (0,T) \\ \mathbf{u}(\mathbf{x},t) & = \mathbf{g}(\mathbf{x},t) \quad (\mathbf{x},t) \in \Gamma \times (0,T) \\ \mathbf{u}(\mathbf{x},0) & = \mathbf{u}_0(\mathbf{x}) \quad \mathbf{x} \in \Omega^e \\ \mathbf{u}_t(\mathbf{x},0) & = \mathbf{v}_0(\mathbf{x}) \quad \mathbf{x} \in \Omega^e, \end{cases} \tag{1}$$

where $\rho > 0$ is the constant material density, $\lambda > 0$ and $\mu > 0$ are the Lamé constants.

The time-domain boundary integral equation (TDBIE) for the displacement $\mathbf{u}(\mathbf{x},t)$ of Problem (1) with $\mathbf{f} = (\mathrm{f}_1, \mathrm{f}_2)$, $\mathbf{g} = (\mathrm{g}_1, \mathrm{g}_2)$, $\mathbf{u}_0 = (\mathrm{u}_{1,0}, \mathrm{u}_{2,0})$ and $\mathbf{v}_0 = (\mathrm{v}_{1,0}, \mathrm{v}_{2,0})$, is formulated in a usual manner as

$$\sum_{\ell=1}^{2} \int_0^t \int_\Gamma U^*_{i\ell}(\mathbf{x}-\mathbf{y}, t-s)\mathrm{t}_\ell(\mathbf{y},s)\,\mathrm{d}\Gamma_{\mathbf{y}}\mathrm{d}s \; - \sum_{\ell=1}^{2} \int_0^t \int_\Gamma T^*_{i\ell}(\mathbf{x}-\mathbf{y}, t-s)\mathrm{u}_\ell(\mathbf{y},s)\,\mathrm{d}\Gamma_{\mathbf{y}}\mathrm{d}s$$

$$+ I_{\mathrm{u}_{i,0}}(\mathbf{x},t) \; + I_{\mathrm{v}_{i,0}}(\mathbf{x},t) + I_{\mathrm{f}_i}(\mathbf{x},t) = \begin{cases} \mathrm{u}_i(\mathbf{x},t) & \mathbf{x} \in \Omega^e \quad (2a) \\ \dfrac{1}{2}\mathrm{u}_i(\mathbf{x},t) & \mathbf{x} \in \Gamma \quad (2b) \end{cases}$$

where $U^*_{i\ell}$ and $T^*_{i\ell}$, $i = 1, 2$, are the displacement and traction fundamental solutions, respectively, and t_ℓ is the ℓ-component of the traction vector $\mathbf{t}$ associated with $\mathbf{u}$. The expression of

$U^*_{i\ell}$ and $T^*_{i\ell}$ can be found in [18], while the volume integrals are defined by

$$
\begin{aligned}
I_{\mathrm{u}_{i,0}}(\mathbf{x},t) &:= \sum_{\ell=1}^{2} \frac{\partial}{\partial t} \int_{\Omega^e} U^*_{i\ell}(\mathbf{x}-\mathbf{y},t)\mathrm{u}_{\ell,0}(\mathbf{y},t)\mathrm{d}\mathbf{y} \\
I_{\mathrm{v}_{i,0}}(\mathbf{x},t) &:= \sum_{\ell=1}^{2} \int_{\Omega^e} U^*_{i\ell}(\mathbf{x}-\mathbf{y},t)\mathrm{v}_{\ell,0}(\mathbf{y},t)\mathrm{d}\mathbf{y} \\
I_{\mathrm{f}_i}(\mathbf{x},t) &:= \sum_{\ell=1}^{2} \int_0^t \int_{\Omega^e} U^*_{i\ell}(\mathbf{x}-\mathbf{y},t-s)\mathrm{f}_\ell(\mathbf{y},s)\mathrm{d}\mathbf{y}\mathrm{d}s.
\end{aligned}
\tag{3}
$$

The details of the TDBIE reformulations (2a)-(2b) of Problem (1) can be found, for example, in [17, 4].

In this paper we assume that the problem data satisfy the smoothness and compatibility conditions which guarantee the solution $\mathbf{u}(\mathbf{x},t)$ to be at least C^2 continuous in $\overline{\Omega^e}\times[0,T]$.

2.1 Numerical resolution of the standard TDBIE formulation

In this section, we describe the numerical procedure we adopt to solve (2b) in the unknowns t_ℓ, $\ell=1,2$, being $\mathrm{u}_\ell=\mathrm{g}_\ell$ known on Γ. Once the solution $\mathbf{t}=(\mathrm{t}_1,\mathrm{t}_2)$ is retrieved, the displacement $\mathbf{u}(\mathbf{x},t)$ is computed at any exterior point $\mathbf{x}$ of Ω^e and at any time t by using (2a).

For the solution of (2b), we consider the numerical approach which combines the time integral discretization by using a Lubich second-order time convolution quadrature (see [11]), recalled in the Appendix, with a (continuous) piecewise linear space collocation method.

2.1.1 Time discretization

We consider a uniform partition of the interval $[0,T]$ into N steps of equal length $\Delta_t=T/N$ and we collocate equations (2b) at the time instants $t_n=n\Delta_t$, $n=0,\dots,N$. After having exchanged the order of integration, we approximate the time integrals by means of (A1) (see Appendix for details). Then, setting $\widehat{U}^*_{i\ell}(r)) := \widehat{U}^*_{i\ell}(r,s)$, $\widehat{T}^*_{i\ell}(r)) := \widehat{T}^*_{i\ell}(r,s)$, we obtain the following integral equations on Γ: for $i=1,2$ and $n=0,\dots,N$

$$
\begin{aligned}
\sum_{\ell=1}^{2}\sum_{j=0}^{n} \int_\Gamma \omega_{n-j}(\Delta_t;\widehat{U}^*_{i\ell}(r))\,\mathrm{t}^j_\ell(\mathbf{y})\,\mathrm{d}\Gamma_{\mathbf{y}} \;=& \frac{1}{2}\mathrm{g}^n_i(\mathbf{x}) + \sum_{\ell=1}^{2}\sum_{j=0}^{n} \int_\Gamma \omega_{n-j}(\Delta_t;\widehat{T}^*_{i\ell}(r))\,\mathrm{g}^j_\ell(\mathbf{y})\,\mathrm{d}\Gamma_{\mathbf{y}} \\
& - I_{\mathrm{u}_{i,0}}(\mathbf{x},t_n) - I_{\mathrm{v}_{i,0}}(\mathbf{x},t_n) - I_{\mathrm{f}_i}(\mathbf{x},t_n)
\end{aligned}
\tag{4}
$$

in the unknowns $\mathrm{t}^n_\ell(\mathbf{x}) \approx \mathrm{t}_\ell(\mathbf{x},t_n)$, with $r=\|\mathbf{x}-\mathbf{y}\|$. In (4) $\omega_{n-j}(\Delta_t;\widehat{W}^*_{i\ell}(r))$ denotes the quadrature coefficient associated with the Laplace transform of the convolution kernel $W^*_{i\ell}=U^*_{i\ell},T^*_{i\ell}$, which is then approximated by formula (A3).

The expressions of the Laplace transforms $\widehat{W}^*_{i\ell}$, involved in (A3), can be found in [4] and are reported here for completeness. These are:

$$
\widehat{U}^*_{i\ell}(r,s) = \frac{1}{2\pi\rho v_S^2}\Big(\psi(r,s)\delta_{i\ell} - \chi(r,s)r_{,i}r_{,\ell}\Big) \tag{5}
$$

$$
\begin{aligned}
\widehat{T}^*_{i\ell}(r,s) =& \frac{1}{2\pi}\left\{\left[\frac{\partial\psi}{\partial r}(r,s) - \frac{\chi(r,s)}{r}\right]\left(\delta_{i\ell}\frac{\partial r}{\partial\mathbf{n}} + r_{,\ell}n_i\right) - 2\frac{\chi(r,s)}{r}\left(r_{,i}n_\ell - 2r_{,i}r_{,\ell}\frac{\partial r}{\partial\mathbf{n}}\right)\right. \\
& \left. -2\frac{\partial\chi}{\partial r}(r,s)r_{,i}r_{,\ell}\frac{\partial r}{\partial\mathbf{n}} + \left(\frac{v_P^2}{v_S^2}-2\right)\left[\frac{\partial\psi}{\partial r}(r,s) - \frac{\partial\chi}{\partial r}(r,s) - \frac{\chi(r,s)}{r}\right]r_{,i}n_\ell\right\},
\end{aligned}
\tag{6}
$$

where $r_{,i} := \partial_{y_i} r$, $\delta_{i\ell}$ is the Kronecker delta and v_P, v_S denote the so-called P- and S-wave speeds defined by (see Section 3)

$$v_P = \sqrt{\frac{\lambda + 2\mu}{\rho}}, \qquad v_S = \sqrt{\frac{\mu}{\rho}}. \tag{7}$$

The functions ψ and χ in (5) and (6) are defined as follows:

$$\psi(r,s) = K_0\left(\frac{rs}{v_S}\right) + \left(\frac{v_S}{rs}\right)\left[K_1\left(\frac{rs}{v_S}\right) - \frac{v_S}{v_P}K_1\left(\frac{rs}{v_P}\right)\right], \tag{8}$$

$$\chi(r,s) = K_2\left(\frac{rs}{v_S}\right) - \left(\frac{v_S}{v_P}\right)^2 K_2\left(\frac{rs}{v_P}\right), \tag{9}$$

where K_0, K_1 and K_2 are the second-kind modified Bessel functions of order 0, 1 and 2, respectively.

By using the relations $K_0'(z) = -K_1(z)$, $K_1'(z) = -K_0(z) - 1/zK_1(z)$ and $K_2'(z) = -2/zK_2(z) - K_1(z)$, easy calculations yield (see [9])

$$\frac{\partial \psi}{\partial r}(r,s) = -\frac{1}{r}\left[\chi(r,s) + \frac{rs}{v_S}K_1\left(\frac{rs}{v_S}\right)\right] \tag{10}$$

and

$$\frac{\partial \chi}{\partial r}(r,s) = -\frac{1}{r}\left[\frac{rs}{v_S}K_1\left(\frac{rs}{v_S}\right) - \left(\frac{v_S}{v_P}\right)^2 \frac{rs}{v_P}K_1\left(\frac{rs}{v_P}\right) + 2\chi(r,s)\right]. \tag{11}$$

2.1.2 Space discretization

In order to describe the space discretization, we assume that the boundary Γ is defined, for simplicity, by a global (C^3-continuous) parametric representation

$$\mathbf{x} = \boldsymbol{\eta}(\vartheta) = (\eta_1(\vartheta), \eta_2(\vartheta)), \qquad \vartheta \in [0,1]. \tag{12}$$

After having introduced the parametric representation (12), hence reduced the integration on Γ into the equivalent one defined on the parametrization interval $[0,1]$, we apply a nodal collocation boundary element method with piecewise linear basis functions $\{N_k\}_{k=1}^{M+1}$ associated to a uniform partition $\{\vartheta_k\}_{k=1}^{M+1}$ of $[0,1]$.

By approximating the unknown functions $\mathrm{t}_\ell^n(\mathbf{x})$, $\ell = 1,2$, for $\mathbf{x} \in \Gamma$ by

$$\mathrm{t}_\ell^j(\boldsymbol{\eta}(\vartheta)) \approx \sum_{k=1}^{M+1} \mathrm{t}_{\ell,k}^j N_k(\vartheta), \tag{13}$$

we end up with the following block lower triangular Toeplitz system

$$\sum_{\ell=1}^{2}\sum_{j=0}^{n} \mathbf{U}_{i\ell}^{n-j}\mathbf{t}_\ell^j = \frac{1}{2}\mathbf{g}_i^n + \sum_{\ell=1}^{2}\sum_{j=0}^{n} \mathbf{T}_{i\ell}^{n-j}\mathbf{g}_\ell^j - \mathbf{I}_{\mathrm{u}_{i,0}}^n - \mathbf{I}_{\mathrm{v}_{i,0}}^n - \mathbf{I}_{\mathrm{f}_i}^n =: \mathbf{b}_i^n, \quad i = 1,2 \tag{14}$$

in the unknowns $\mathbf{t}_\ell^n = (t_{\ell,1}^n, \ldots, t_{\ell,M+1}^n)^T$, with $\ell = 1,2$ and $n = 0, \ldots, N$. The entries of the matrices $\mathbf{U}_{i\ell}^n$ and $\mathbf{T}_{i\ell}^n$ in (14) are

$$(\mathbf{U}_{i\ell}^n)_{m,k} = \frac{1}{2\pi}\frac{\varrho^{-n}}{L}\sum_{l=0}^{L-1}\left(\int_0^1 \widehat{U}_{i\ell}^*(r_m, z)\, N_k(\vartheta)\, \|\boldsymbol{\eta}'(\vartheta)\|\, \mathrm{d}\vartheta\right) \mathrm{e}^{-\frac{\imath n l 2\pi}{L}} \tag{15}$$

and

$$(\mathbf{T}_{i\ell}^n)_{m,k} = \frac{1}{2\pi}\frac{\varrho^{-n}}{L}\sum_{l=0}^{L-1}\left(\int_0^1 \widehat{T}_{i\ell}^*\left(r_m, z\right) N_k(\vartheta)\,\|\boldsymbol{\eta}'(\vartheta)\|\,\mathrm{d}\vartheta\right)\mathrm{e}^{-\frac{\imath n l 2\pi}{L}}, \tag{16}$$

where $z := \gamma(\varrho \mathrm{e}^{il2\pi/L})/\Delta_t$, $r_m = \|\boldsymbol{\eta}(\vartheta_m) - \boldsymbol{\eta}(\vartheta)\|$, being ϑ_m, $m = 1, \ldots, M+1$, the collocation points.

In matrix form, the solution of system (14) at each time instant $t = t_n$ is determined by solving the following 2×2 block linear system

$$\begin{pmatrix} \mathbf{U}_{11}^0 & \mathbf{U}_{12}^0 \\ \\ \mathbf{U}_{21}^0 & \mathbf{U}_{22}^0 \end{pmatrix} \begin{pmatrix} \mathbf{t}_1^n \\ \\ \mathbf{t}_2^n \end{pmatrix} = -\sum_{j=0}^{n-1} \begin{pmatrix} \mathbf{U}_{11}^{n-j} & \mathbf{U}_{12}^{n-j} \\ \\ \mathbf{U}_{21}^{n-j} & \mathbf{U}_{22}^{n-j} \end{pmatrix} \begin{pmatrix} \mathbf{t}_1^j \\ \\ \mathbf{t}_2^j \end{pmatrix} + \begin{pmatrix} \mathbf{b}_1^n \\ \\ \mathbf{b}_2^n \end{pmatrix}. \tag{17}$$

for $n = 0, \ldots, N$.

2.1.3 Efficient computation of the matrix elements

In order to compute accurately the integrals appearing in (15) and (16), it is important to make some preliminary remarks on the behaviour of the involved integrand functions.

We start by detailing the numerical procedure to compute the matrix entries of $\mathbf{U}_{i\ell}^n$. To this aim, we rewrite (8) as follows

$$\psi(r, s) = K_0\left(\frac{rs}{v_S}\right) + \psi_1(r, s), \tag{18}$$

where

$$\psi_1(r, s) := \left(\frac{v_S}{rs}\right) K_1\left(\frac{rs}{v_S}\right) - \left(\frac{v_S}{v_P}\right)^2 \left(\frac{v_P}{rs}\right) K_1\left(\frac{rs}{v_P}\right).$$

We recall the series expansion of the Bessel function K_0 appearing in (18) (see [1] formula (9.6.13)):

$$\begin{aligned} K_0(z) &= -\left(\ln\frac{z}{2} + \gamma\right) I_0(z) + \sum_{k=1}^{\infty} a_k \frac{\left(z^2/4\right)^k}{(k!)^2} \\ I_0(z) &= \sum_{k=0}^{\infty} \frac{\left(z^2/4\right)^k}{(k!)^2}, \quad a_1 = 1,\ a_{k+1} = a_k + \frac{1}{k+1}, \end{aligned} \tag{19}$$

$\gamma = 0.5772156649...$ being the well known Euler's constant. Formula (19) highlights the log-behaviour of the first term in ψ for small values of z. Moreover, the remaining term ψ_1 in (18) involves two functions of the form $K_1(z)/z$ which, separately, are hypersingular. However, these hypersingularities are only apparent because, by properly manipulating the expressions therein, the hypersingularities cancel each other out and the overall sum has only a log-singularity. Indeed, by using the series expansion of the Bessel function $K_1(z)$ (see [1] formula (9.6.11))

$$K_1(z) = \frac{1}{z} + \log\left(\frac{z}{2}\right)\frac{z}{2} + \frac{z}{2}\left\{\log\left(\frac{z}{2}\right)\sum_{k=1}^{\infty}\frac{(z^2/4)^k}{k!(k+1)!} - \frac{1}{2}\sum_{k=0}^{\infty}\left[\Psi(k+1) + \Psi(k+2)\right]\frac{(z^2/4)^k}{k!(k+1)!}\right\}$$

with $\Psi(k) = -\gamma + \sum_{n=1}^{k-1} \frac{1}{n}$ defined by (6.3.2) in [1], easy calculations yield

$$\psi_1(r,s) = \frac{1}{2}\left[\log\left(\frac{rs}{2v_S}\right) - \left(\frac{v_S}{v_P}\right)^2 \log\left(\frac{rs}{2v_P}\right)\right] + \frac{1}{2}\left[R\left(\frac{rs}{v_S}\right) - \left(\frac{v_S}{v_P}\right)^2 R\left(\frac{rs}{v_P}\right)\right] \tag{20}$$

where

$$R(z) = -\frac{1}{2}\left[\Psi(1) + \Psi(2)\right] + \sum_{k=1}^{\infty}\left\{\log\left(\frac{z}{2}\right) - \frac{1}{2}\left[\Psi(k+1) + \Psi(k+2)\right]\right\}\frac{(z^2/4)^k}{k!(k+1)!}. \tag{21}$$

Therefore, by taking into account (19), (20) and (21), we can state that the overall behaviour of the function ψ in (18) is of log-type.

For what concerns the expression of χ in (9), we remark that $K_2(z)$ is hypersingular at $z = 0$. However, by using the relation $K_2(z) = K_0(z) + 2K_1(z)/z$, we can rewrite χ as follows:

$$\chi(r,s) = K_0\left(\frac{rs}{v_S}\right) - \left(\frac{v_S}{v_P}\right)^2 K_0\left(\frac{rs}{v_P}\right) + 2\psi_1(r,s), \tag{22}$$

where some log-singularities formally appear. However these cancel each other out after inserting in (22) the series expansions (19) and (20). Indeed we obtain:

$$\chi(r,s) = \gamma\left[\left(\frac{v_S}{v_P}\right)^2 - 1\right] + R\left(\frac{rs}{v_S}\right) - \left(\frac{v_S}{v_P}\right)^2 R\left(\frac{rs}{v_P}\right) + R_1\left(\frac{rs}{v_S}\right) - \left(\frac{v_S}{v_P}\right)^2 R_1\left(\frac{rs}{v_P}\right), \tag{23}$$

where

$$R_1(z) = \sum_{k=1}^{\infty}\left\{-\left[\log\left(\frac{z}{2}\right) + \gamma\right] + a_k\right\}\frac{(z^2/4)^k}{(k!)^2}. \tag{24}$$

Therefore, we can conclude that actually the function χ tends to zero as $z \to 0$.

For what concerns the computation of the entries of the matrices $\mathbf{T}^n_{i\ell}$, by taking into account (10) and (11), we can rewrite (6) as follows:

$$\begin{aligned}
\widehat{T}^*_{i\ell}(r,s) =& \frac{1}{2\pi}\left\{\left[\left(\frac{\partial\psi}{\partial r}(r,s) - \frac{\chi(r,s)}{r}\right)\delta_{i\ell} + \left(4\frac{\chi(r,s)}{r} - 2\frac{\partial\chi}{\partial r}(r,s)\right) r_{,i}r_{,\ell}\right]\frac{\partial r}{\partial \mathbf{n}}\right. \\
&+ \left[\frac{\partial\psi}{\partial r}(r,s) - \frac{\chi(r,s)}{r}\right] r_{,\ell}n_i \\
&\left.+ \left[\left(\frac{v_P^2}{v_S^2} - 2\right)\left(\frac{\partial\psi}{\partial r}(r,s) - \frac{\partial\chi}{\partial r}(r,s) - \frac{\chi(r,s)}{r}\right) - 2\frac{\chi(r,s)}{r}\right] r_{,i}n_\ell\right\} \\
=& (\mathcal{T}_1)_{i\ell}(r,s) + (\mathcal{T}_2)_{i\ell}(r,s)
\end{aligned} \tag{25}$$

where

$$\begin{aligned}
(\mathcal{T}_1)_{i\ell}(r,s) :=& \frac{1}{2\pi}\left\{-\left[2\chi(r,s) + \frac{rs}{v_S}K_1\left(\frac{rs}{v_S}\right)\right]\delta_{i\ell}\right. \\
&\left.+ \left[8\chi(r,s) + 2\frac{rs}{v_S}K_1\left(\frac{rs}{v_S}\right) - 2\left(\frac{v_S}{v_P}\right)^2\frac{rs}{v_P}K_1\left(\frac{rs}{v_P}\right)\right] r_{,i}r_{,\ell}\right\}\frac{1}{r}\frac{\partial r}{\partial \mathbf{n}}
\end{aligned} \tag{26}$$

and

$$(\mathcal{T}_2)_{i\ell}(r,s) := -\frac{1}{2\pi}\left\{\left[2\chi(r,s)+\frac{rs}{v_S}K_1\left(\frac{rs}{v_S}\right)\right]r_{,\ell}n_i \right. \\ \left. + \left[2\chi(r,s)+\frac{rs}{v_P}K_1\left(\frac{rs}{v_P}\right)-2\left(\frac{v_S}{v_P}\right)^2\frac{rs}{v_P}K_1\left(\frac{rs}{v_P}\right)\right]r_{,i}n_\ell\right\}\frac{1}{r}. \tag{27}$$

Noting that $\partial r/\partial \mathbf{n} \sim r$ for $r \to 0$, and recalling the previous statements, the term $(\mathcal{T}_1)_{i\ell}$ turns out to be integrable in the classic sense. On the contrary, the term $(\mathcal{T}_2)_{i\ell}$ has a singularity of the type r^{-1} as $r \to 0$; thus the corresponding integral has to be defined in the Cauchy principal value sense and properly treated.

Because of the above remarks, to compute the matrix entries $(\mathbf{U}^n_{i\ell})_{m,k}$ and $(\mathbf{T}^n_{i\ell})_{m,k}$ we proceed as follows. When r_m is smaller than a prescribed tolerance ε_m, to efficiently compute the integrals having the kernels $\widehat{U}^*_{i\ell}$ and $\widehat{T}^*_{i\ell}$, we have first to take into account the behaviours of the kernel single components given in (8)–(11) and, using the series expansions of the latter, cancel their apparent higher order singularities. After this analytic cancelation, the remaining singularities are of the type $\log r_m$ for $\widehat{U}^*_{i\ell}$ and r_m^{-1} for $\widehat{T}^*_{i\ell}$.

To compute the integrals having the log term, we apply the very simple and efficient polynomial smoothing technique proposed in [15] and [16], coupled with a ν-point Gauss-Legendre quadrature rule. The series in (21) and (24) are truncated to $k = N_0$, for a suitable N_0. In the simpler case where r_m is larger than the prescribed tolerance ε_m, to compute the integrals in (15) we directly apply to them the above chosen ν-point Gauss-Legendre rule; the evaluation of their kernel functions are performed using directly expressions (8)–(11).

For what concerns the integrals in (16), by taking into account the behaviour of $\widehat{T}^*_{i\ell}$ given by (25)–(27), the integrals containing the regular terms $(\mathcal{T}_1)_{i\ell}$, and $(\mathcal{T}_2)_{i\ell}$ for $k \neq m$, are computed by the ν-point Gauss-Legendre rule. On the contrary, for the evaluation of the matrix elements defined by (16) with $k = m$, and in particular those having the kernel singular component $\mathcal{T}_2$ (see (27)), we proceed as follows. First we split the integration interval in two parts

$$\fint_0^1 (\mathcal{T}_2)_{i\ell}\,(r_m,s)\,N_m(\vartheta)\,\|\boldsymbol{\eta}'(\vartheta)\|\mathrm{d}\vartheta = \left(\fint_{\vartheta_{m-1}}^{\vartheta_m} + \fint_{\vartheta_m}^{\vartheta_{m+1}}\right)\frac{f_{i\ell}\,(\vartheta)}{r_m}\mathrm{d}\vartheta, \quad r_m = \|\boldsymbol{\eta}(\vartheta_m)-\boldsymbol{\eta}(\vartheta)\|$$

where $f_{i\ell}(\vartheta) = (\mathcal{T}_2)_{i\ell}\,(r_m,s)\,N_m(\vartheta)\,\|\boldsymbol{\eta}'(\vartheta)\|r_m$ denotes the smooth part of the integrand function; then, following [14], we compute the hypersingular integrals as follows:

$$\begin{aligned} &\int_{\vartheta_{m-1}}^{\vartheta_m} \frac{f_{i\ell}\,(\vartheta)\,(\vartheta_m-\vartheta)/r_m - f^-_{i\ell}}{\vartheta_m-\vartheta}\,\mathrm{d}\vartheta \;+\; f^-_{i\ell}\log(\vartheta_m-\vartheta_{m-1}), \\ &\int_{\vartheta_m}^{\vartheta_{m+1}} \frac{f_{i\ell}\,(\vartheta)\,(\vartheta-\vartheta_m)/r_m - f^+_{i\ell}}{\vartheta-\vartheta_m}\,\mathrm{d}\vartheta \;+\; f^+_{i\ell}\log(\vartheta_{m+1}-\vartheta_m), \end{aligned} \tag{28}$$

with $f^\pm_{i\ell} = \pm\lim_{\vartheta\to\vartheta_m^\pm} f_{i\ell}\,(\vartheta)\,(\vartheta-\vartheta_m)/r_m$. Finally, the regular integrals in (28) are computed by using the same ν-point Gauss-Legendre rule already used for the preceding integrals.

Further details on the choice of the number of quadrature points ν and on the parameters ε_m and N_0 are given in Section 4.

Remark 2.1 *We recall that (see [8]) the efficient and accurate evaluation of all the integrals required by the proposed method is a key ingredient for its success. In particular, the more*

accurate is the integral evaluation, the larger is the length of the time integration interval that one can choose, whenever this is needed (see Example 3).

We further note that once the BIE has been solved, the (unknown) $\mathbf{u}(\mathbf{x},t)$ *is evaluated at a point* $\mathbf{x}\in\Omega^e$ *by using its representation* (2a)*, whose kernels are all smooth functions. However, for* $\mathbf{x}$ *very closed to the boundary* Γ*, these kernels have quasi-singularities that have to be properly treated.*

3 A novel approach

It is well-known (see [5]) that under the assumptions we have previously made on the domain boundary Γ and on the problem data, by taking first the divergence and then the **curl** of the elastodynamic equation in $\mathbb{R}^3$, we can always replace the unknown displacement by two unknown potentials, the first scalar and the second vectorial, φ_P and $\boldsymbol{\varphi}_S$, solutions of the following two wave equations:

$$\begin{cases} \dfrac{\partial^2\varphi_P}{\partial t^2}(\mathbf{x},t)-v_P^2\nabla^2\varphi_P(\mathbf{x},t) &= \dfrac{1}{\rho}\mathrm{f}_P(\mathbf{x},t) \\ \\ \dfrac{\partial^2\boldsymbol{\varphi}_S}{\partial t^2}(\mathbf{x},t)-v_S^2\nabla^2\boldsymbol{\varphi}_S(\mathbf{x},t) &= \dfrac{1}{\rho}\mathbf{f}_S(\mathbf{x},t), \end{cases} \tag{29}$$

where $\mathbf{f}=\nabla\mathrm{f}_P+\mathbf{curl}\,\mathbf{f}_S$ and $\mathbf{u}=\nabla\varphi_P+\mathbf{curl}\,\boldsymbol{\varphi}_S=:\mathbf{u}_P+\mathbf{u}_S$. The unknowns φ_P and $\boldsymbol{\varphi}_S$ are called Primary (or longitudinal) and Secondary (or transverse) waves, since, being always $v_P>v_S$, the first travel faster. The vector fields $\mathbf{u}_P,\mathbf{u}_S$ denote the corresponding displacement components.

This is the well-known Helmholtz decomposition of a vector field, which is used in many applications of Physics. Formulation (29) is of particular interest, for example, when the problem source is a P-wave or a S-wave, and the knowledge of the propagation of the P- and S-waves generated by this source is required. However, this approach requires corresponding boundary conditions for system (29), which must couple the two wave equations. This is the major issue for the application of this alternative approach. For example, when the interior domain Ω^i is a cavity, a null traction must be imposed on Γ. But this means to use the representation of the traction in terms of φ_P and $\boldsymbol{\varphi}_S$, which involves the evaluation of all second order partial derivatives of the latter two functions, a computation that turns out to be costly.

In the 2D case mentioned in the first paragraph of the introduction, after defining the new operators

$$\mathbf{curl}\;w=\begin{pmatrix}\partial_{x_2}w\\ -\partial_{x_1}w\end{pmatrix},\qquad\qquad \mathrm{curl}\,\mathbf{u}=\partial_{x_1}\mathrm{u}_2-\partial_{x_2}\mathrm{u}_1,$$

the following alternative expression of (1) is obtained (see [3]):

$$\begin{cases} \rho\,\dfrac{\partial^2\mathbf{u}}{\partial t^2}(\mathbf{x},t)-(\lambda+2\mu)\nabla(\mathrm{div}\,\mathbf{u})(\mathbf{x},t)+\mu\,\mathbf{curl}\,(\mathrm{curl}\,\mathbf{u})(\mathbf{x},t)=\mathbf{f}(\mathbf{x},t), & (\mathbf{x},t)\in\ \Omega^e\times(0,T)\\ \mathbf{u}(\mathbf{x},t)=\mathbf{g}(\mathbf{x},t) & (\mathbf{x},t)\in\ \Gamma\times(0,T)\\ \mathbf{u}(\mathbf{x},0)=\mathbf{u}_0(\mathbf{x}) & \mathbf{x}\in\ \Omega^e\\ \mathbf{u}_t(\mathbf{x},0)=\mathbf{v}_0(\mathbf{x}) & \mathbf{x}\in\ \Omega^e. \end{cases} \tag{30}$$

Note that this new problem representation is the 2D analogue of the corresponding 3D one we are considering in this paper.

In the same paper [3], by proceeding as in the 3D case, and taking into account the identities

$$-\nabla^2 u = -\mathrm{div}\,(\nabla u) = \mathrm{curl}\,(\mathbf{curl}\,u), \quad \mathrm{div}\,(\mathbf{curl}\,u) = 0, \quad \mathrm{curl}\,(\nabla u) = 0, \tag{31}$$

the following decoupled equations have then been obtained:

$$\begin{cases} \dfrac{\partial^2 \varphi_P}{\partial t^2}(\mathbf{x},t) - v_P^2 \nabla^2 \varphi_P(\mathbf{x},t) &= \dfrac{1}{\rho}\mathrm{f}_P(\mathbf{x},t) \\ \\ \dfrac{\partial^2 \varphi_S}{\partial t^2}(\mathbf{x},t) - v_S^2 \nabla^2 \varphi_S(\mathbf{x},t) &= \dfrac{1}{\rho}\mathrm{f}_S(\mathbf{x},t) \end{cases} \tag{32}$$

where now also φ_S is a scalar function and $\mathbf{f} = \nabla \mathrm{f}_P + \mathbf{curl}\,\mathrm{f}_S$.

The two equations in (32) are however coupled on the boundary Γ by the problem Dirichlet condition. This takes the new form

$$\nabla \varphi_P + \mathbf{curl}\,\varphi_S = \mathbf{g} \qquad \text{on } \Gamma. \tag{33}$$

With reference to the domain Ω^i, we introduce along Γ, anti-clockwise oriented, the ingoing unit normal vector $\mathbf{n} = (n_1, n_2)^T$ and the corresponding unit tangent vector $\boldsymbol{\tau} = (n_2, -n_1)^T$, so that the identities

$$\frac{\partial \phi}{\partial \mathbf{n}} = \nabla \phi \cdot \mathbf{n}, \qquad \frac{\partial \phi}{\partial \boldsymbol{\tau}} = \nabla \phi \cdot \boldsymbol{\tau}$$

hold on Γ for any smooth enough scalar function ϕ.

Following [3], by applying the scalar products, first by $\mathbf{n}$ and then by $\boldsymbol{\tau}$, to both sides of (33), hence using the following identities:

$$\mathbf{curl}\,\phi \cdot \mathbf{n} = -\frac{\partial \phi}{\partial \boldsymbol{\tau}}, \qquad \mathbf{curl}\,\phi \cdot \boldsymbol{\tau} = \frac{\partial \phi}{\partial \mathbf{n}} \qquad \text{on } \Gamma,$$

the relations

$$\frac{\partial \varphi_P}{\partial \mathbf{n}} - \frac{\partial \varphi_S}{\partial \boldsymbol{\tau}} = \mathbf{g} \cdot \mathbf{n}, \qquad \frac{\partial \varphi_S}{\partial \mathbf{n}} + \frac{\partial \varphi_P}{\partial \boldsymbol{\tau}} = \mathbf{g} \cdot \boldsymbol{\tau} \qquad \text{on } \Gamma \tag{34}$$

are obtained.

Finally, after setting

$$\begin{array}{rclrcl} \varphi_{P,0}(\mathbf{x}) &:=& \varphi_P(\mathbf{x},0), & \varphi_{S,0}(\mathbf{x}) &:=& \varphi_S(\mathbf{x},0) \\ \bar{\varphi}_{P,0}(\mathbf{x}) &:=& \partial_t \varphi_P(\mathbf{x},0), & \bar{\varphi}_{S,0}(\mathbf{x}) &:=& \partial_t \varphi_S(\mathbf{x},0) \end{array} \tag{35}$$

and decomposing the initial data $\mathbf{u}_0$, $\mathbf{v}_0$ and the Dirichlet datum as follows

$$\begin{array}{rcl} \mathbf{u}_0(\mathbf{x}) &=& \nabla \varphi_{P,0}(\mathbf{x}) + \mathbf{curl}\,\varphi_{S,0}(\mathbf{x}) \\ \mathbf{v}_0(\mathbf{x}) &=& \nabla \bar{\varphi}_{P,0}(\mathbf{x}) + \mathbf{curl}\,\bar{\varphi}_{S,0}(\mathbf{x}) \end{array} \tag{36}$$

$$\mathbf{g}(\mathbf{x},t) = \nabla \mathrm{g}_P(\mathbf{x},t) + \mathbf{curl}\,\mathrm{g}_S(\mathbf{x},t), \tag{37}$$

we obtain that the elastodynamics problem (1) is formally equivalent (see [3]) to the following potentials problem:

$$\begin{cases} \dfrac{\partial^2\varphi_P}{\partial t^2} - v_P^2\nabla^2\varphi_P = \dfrac{1}{\rho}\mathrm{f}_P & (\mathbf{x},t)\in\Omega^e\times(0,T) \quad (38a)\\ \dfrac{\partial^2\varphi_S}{\partial t^2} - v_S^2\nabla^2\varphi_S = \dfrac{1}{\rho}\mathrm{f}_S & (\mathbf{x},t)\in\Omega^e\times(0,T) \quad (38b)\\ \dfrac{\partial\varphi_P}{\partial\mathbf{n}} = \dfrac{\partial\varphi_S}{\partial\boldsymbol{\tau}} + \mathbf{g}\cdot\mathbf{n} =: \dfrac{\partial\varphi_S}{\partial\boldsymbol{\tau}} + g_{\mathbf{n}} & (\mathbf{x},t)\in\Gamma\times(0,T) \quad (38c)\\ \dfrac{\partial\varphi_S}{\partial\mathbf{n}} = -\dfrac{\partial\varphi_P}{\partial\boldsymbol{\tau}} + \mathbf{g}\cdot\boldsymbol{\tau} =: -\dfrac{\partial\varphi_P}{\partial\boldsymbol{\tau}} + g_{\boldsymbol{\tau}} & (\mathbf{x},t)\in\Gamma\times(0,T) \quad (38d)\\ \varphi_P(\mathbf{x},0) = \varphi_{P,0}(\mathbf{x}) & \mathbf{x}\in\Omega^e \quad (38e)\\ \varphi_S(\mathbf{x},0) = \varphi_{S,0}(\mathbf{x}) & \mathbf{x}\in\Omega^e \quad (38f)\\ \dfrac{\partial\varphi_P}{\partial t}(\mathbf{x},0) = \bar{\varphi}_{P,0}(\mathbf{x}) & \mathbf{x}\in\Omega^e \quad (38g)\\ \dfrac{\partial\varphi_S}{\partial t}(\mathbf{x},0) = \bar{\varphi}_{S,0}(\mathbf{x}) & \mathbf{x}\in\Omega^e. \quad (38h) \end{cases}$$

Note that, if we consider the Helmholtz decomposition (37) of the datum g, the functions $g_{\mathbf{n}}$ and $g_{\boldsymbol{\tau}}$ are given by

$$g_{\mathbf{n}}(\mathbf{x},t) = \frac{\partial \mathrm{g}_P}{\partial\mathbf{n}}(\mathbf{x},t) - \frac{\partial \mathrm{g}_S}{\partial\boldsymbol{\tau}}(\mathbf{x},t)$$
$$g_{\boldsymbol{\tau}}(\mathbf{x},t) = \frac{\partial \mathrm{g}_P}{\partial\boldsymbol{\tau}}(\mathbf{x},t) + \frac{\partial \mathrm{g}_S}{\partial\mathbf{n}}(\mathbf{x},t).$$

The novel approach we propose to solve elastodynamic problems of form (1) is based on the TDBIE formulation of the above system (38a)-(38h). To this end, we start by recalling the expression of the fundamental solution of the 2D scalar wave equation, related to the propagation of a planar wave travelling with speed c:

$$\frac{\partial^2\varphi}{\partial t^2}(\mathbf{x},t) - c^2\nabla^2\varphi(\mathbf{x},t) = \tilde{f}(\mathbf{x},t). \quad (39)$$

It is well known that the fundamental solution of (39) is given by

$$\widetilde{G}(\mathbf{x},t) = \frac{1}{2\pi c^2}\frac{H\left(t-\dfrac{\|\mathbf{x}\|}{c}\right)}{\sqrt{t^2-\dfrac{\|\mathbf{x}\|^2}{c^2}}}, \quad (40)$$

and satisfies the equation

$$\frac{\partial^2\widetilde{G}}{\partial t^2}(\mathbf{x},t) - c^2\nabla^2\widetilde{G}(\mathbf{x},t) = \delta(\mathbf{x})\delta(t).$$

Proceeding as in [7] and setting $G(\mathbf{x},t) := c^2\widetilde{G}(\mathbf{x},t)$, the following TDBIE for the exterior problem associated to (39) with initial condition $\varphi(\cdot,0)=\varphi_0(\cdot)$ and initial velocity $\varphi_t(\cdot,0) = \overline{\varphi}_0(\cdot)$ can be derived:

$$\int_0^t\int_\Gamma G(\mathbf{x}-\mathbf{y},t-s)\partial_{\mathbf{n}}\varphi(\mathbf{y},s)\,\mathrm{d}\Gamma_{\mathbf{y}}\mathrm{d}s \;-\int_0^t\int_\Gamma \partial_{\mathbf{n}}G(\mathbf{x}-\mathbf{y},t-s)\varphi(\mathbf{y},s)\,\mathrm{d}\Gamma_{\mathbf{y}}\mathrm{d}s$$
$$+\frac{1}{c^2}\frac{\partial}{\partial t}\int_{\Omega^e} G(\mathbf{x}-\mathbf{y},t)\varphi_0(\mathbf{y},t)\mathrm{d}\mathbf{y} \;+\frac{1}{c^2}\int_{\Omega^e} G(\mathbf{x}-\mathbf{y},t)\overline{\varphi}_0(\mathbf{y},t)\mathrm{d}\mathbf{y}$$

$$+\frac{1}{c^2}\int_0^t\int_{\Omega^e} G(\mathbf{x}-\mathbf{y},t-s)\tilde{f}(\mathbf{y},s)\mathrm{d}\mathbf{y}\mathrm{d}s = \begin{cases} \varphi(\mathbf{x},t) & \mathbf{x}\in\Omega^e \quad (41a)\\ \dfrac{1}{2}\varphi(\mathbf{x},t) & \mathbf{x}\in\Gamma. \quad (41b)\end{cases}$$

Therefore, by applying this latter TDBIE representation to both equations (38a) and (38b), and by considering the coupling relations on the boundary Γ (38c) and (38d), we can analogously reformulate (38a)–(38h) as follows:

$$\begin{cases} \dfrac{1}{2}\varphi_P(\mathbf{x},t)+(\mathcal{K}_P\varphi_P)(\mathbf{x},t)-(\mathcal{V}_P(\partial_{\boldsymbol{\tau}}\varphi_S))(\mathbf{x},t) \\ \qquad\qquad = (\mathcal{V}_P\, g_{\mathbf{n}})(\mathbf{x},t)+I_{\varphi_{P,0}}(\mathbf{x},t)+I_{\bar{\varphi}_{P,0}}(\mathbf{x},t)+I_{\mathrm{f}_P}(\mathbf{x},t), \qquad \mathbf{x}\in\Gamma \\ \dfrac{1}{2}\varphi_S(\mathbf{x},t)+(\mathcal{K}_S\varphi_S)(\mathbf{x},t)+(\mathcal{V}_S(\partial_{\boldsymbol{\tau}}\varphi_P))(\mathbf{x},t) \\ \qquad\qquad = (\mathcal{V}_S\, g_{\boldsymbol{\tau}})(\mathbf{x},t)+I_{\varphi_{S,0}}(\mathbf{x},t)+I_{\bar{\varphi}_{S,0}}(\mathbf{x},t)+I_{\mathrm{f}_S}(\mathbf{x},t), \qquad \mathbf{x}\in\Gamma \end{cases} \tag{42}$$

where

$$\begin{aligned}(\mathcal{V}_\star\psi)(\mathbf{x},t) &:= \int_0^t\int_\Gamma G_\star(\mathbf{x}-\mathbf{y},t-s)\psi(\mathbf{y},s)\,\mathrm{d}\Gamma_{\mathbf{y}}\mathrm{d}s \\ (\mathcal{K}_\star\lambda)(\mathbf{x},t) &:= \int_0^t\int_\Gamma G_{\mathbf{n},\star}(\mathbf{x}-\mathbf{y},t-s)\lambda(\mathbf{y},s)\,\mathrm{d}\Gamma_{\mathbf{y}}\mathrm{d}s\end{aligned} \tag{43}$$

are the well known single and double layer operators associated to the scalar wave equation, having set $\star := P, S$ and $G_{\mathbf{n},\star} := \partial_{\mathbf{n}}G_\star$. Moreover

$$\begin{aligned} I_{\varphi_{\star,0}}(\mathbf{x},t) &:= \frac{1}{v_\star^2}\frac{\partial}{\partial t}\int_{\Omega^e} G_\star(\mathbf{x}-\mathbf{y},t)\varphi_{\star,0}(\mathbf{y},t)\mathrm{d}\mathbf{y} \\ I_{\bar{\varphi}_{\star,0}}(\mathbf{x},t) &:= \frac{1}{v_\star^2}\int_{\Omega^e} G_\star(\mathbf{x}-\mathbf{y},t)\bar{\varphi}_{\star,0}(\mathbf{y},t)\mathrm{d}\mathbf{y} \\ I_{\mathrm{f}_\star}(\mathbf{x},t) &:= \frac{1}{\rho v_\star^2}\int_0^t\int_{\Omega^e} G_\star(\mathbf{x}-\mathbf{y},t-s)\mathrm{f}_\star(\mathbf{y},s)\mathrm{d}\mathbf{y}\mathrm{d}s.\end{aligned} \tag{44}$$

are the volume integrals (38e)-(38h) due to the initial data and the body force. In (43) and (44), the fundamental solutions are $G_P(\mathbf{x},t) := v_P^2\widetilde{G}_P(\mathbf{x},t)$ and $G_S(\mathbf{x},t) := v_S^2\widetilde{G}_S(\mathbf{x},t)$, where $\widetilde{G}_P$ and $\widetilde{G}_S$ are given by (40), with c replaced by the velocities v_P and v_S of the P- and S-waves, respectively.

Therefore the potentials problem (38a)-(38h), reformulated in terms of TDBIEs, consists in finding the two scalar functions

$$\varphi_P : \Gamma\times[0,T]\to\mathbb{R} \qquad \text{and} \qquad \varphi_S : \Gamma\times[0,T]\to\mathbb{R}$$

which satisfy the TDBIE system (42). Note that all the data of this new formulation are one order smoother than the corresponding ones in (1).

Remark 3.1 *Once the functions φ_P and φ_S are known, the solution $\mathbf{u} = (\mathrm{u}_1, \mathrm{u}_2)$ of Problem (1) in Ω^e is retrieved from the expression $\mathbf{u} = \nabla\varphi_P + \mathbf{curl}\,\varphi_S$. Indeed, by differentiating (41a) with respect to x_i, for $i = 1, 2$, we obtain*

$$\begin{aligned}\mathrm{u}_1(\mathbf{x},t) &= \partial_{x_1}\varphi_P(\mathbf{x},t)+\partial_{x_2}\varphi_S(\mathbf{x},t) \\ \mathrm{u}_2(\mathbf{x},t) &= \partial_{x_2}\varphi_P(\mathbf{x},t)-\partial_{x_1}\varphi_S(\mathbf{x},t),\end{aligned} \tag{45}$$

where

$$\begin{aligned}\partial_{x_i}\varphi_P(\mathbf{x},t) = &-\int_0^t\int_\Gamma \partial_{x_i}G_{\mathbf{n},P}(\mathbf{x}-\mathbf{y},t-s)\varphi_P(\mathbf{y},s)\,\mathrm{d}\Gamma_{\mathbf{y}}\mathrm{d}s\\ &+\int_0^t\int_\Gamma \partial_{x_i}G_P(\mathbf{x}-\mathbf{y},t-s)\partial_{\boldsymbol{\tau}}\varphi_S(\mathbf{y},s)\,\mathrm{d}\Gamma_{\mathbf{y}}\mathrm{d}s\\ &+\partial_{x_i}\Big[(\mathcal{V}_P\, g_{\mathbf{n}})(\mathbf{x},t)+I_{\varphi_{P,0}}(\mathbf{x},t)+I_{\bar\varphi_{P,0}}(\mathbf{x},t)+I_{\mathrm{f}_P}(\mathbf{x},t)\Big]\end{aligned} \tag{46}$$

and

$$\begin{aligned}\partial_{x_i}\varphi_S(\mathbf{x},t) = &-\int_0^t\int_\Gamma \partial_{x_i}G_{\mathbf{n},S}(\mathbf{x}-\mathbf{y},t-s)\varphi_S(\mathbf{y},s)\,\mathrm{d}\Gamma_{\mathbf{y}}\mathrm{d}s\\ &-\int_0^t\int_\Gamma \partial_{x_i}G_S(\mathbf{x}-\mathbf{y},t-s)\partial_{\boldsymbol{\tau}}\varphi_P(\mathbf{y},s)\,\mathrm{d}\Gamma_{\mathbf{y}}\mathrm{d}s\\ &+\partial_{x_i}\Big[(\mathcal{V}_S\, g_{\boldsymbol{\tau}})(\mathbf{x},t)+I_{\varphi_{S,0}}(\mathbf{x},t)+I_{\bar\varphi_{S,0}}(\mathbf{x},t)+I_{\mathrm{f}_S}(\mathbf{x},t)\Big].\end{aligned} \tag{47}$$

According to Remark 3.2 below, the behaviour of the kernels $\partial_{x_i}G_{\mathbf{n},\star}(r,t-s)$ as $r\to 0$ is $O(r^{-2})$, while that of the remaining two kernels is $O(r^{-1})$. Thus, when $\mathbf{x}$ is very close to the boundary Γ, also these four kernels have quasi-singularities that need to be properly treated.

As we have remarked at the beginning of this section, the major issue for the application of this alternative approach is the determination of the (coupling) boundary conditions of the new problem formulation. For the case where the Dirichlet condition considered in this section is replaced by the null traction, see [12].

3.1 The numerical resolution of the new TDBIE system

Following [7], for the numerical solution of system (42), we propose a numerical approach which combines the time integral discretization by using a Lubich second-order time convolution quadrature (see [11]) with a (continuous) piecewise linear space collocation method.

3.1.1 Time discretization

We start by introducing the time integral discretization by means of the chosen Lubich convolution quadrature. To this end, we first split the interval $[0,T]$ into N steps of equal length $\Delta_t = T/N$ and collocate equations (42) at the times $t_n = n\Delta_t$, $n=0,\dots,N$. After having exchanged the order of integration, the time integrals appearing in the definition of the operators $\mathcal{V}_\star$ and $\mathcal{K}_\star$ in (43) are discretized by means of the Lubich convolution quadrature formula (A1) associated with the BDF2 method:

$$\begin{aligned}(\mathcal{V}_\star\psi)(\mathbf{x},t_n) &\approx \sum_{j=0}^{n}\int_\Gamma \omega_{n-j}\left(\Delta_t; G_\star(r)\right)\psi^j(\mathbf{y})\,\mathrm{d}\Gamma_{\mathbf{y}}\\ (\mathcal{K}_\star\lambda)(\mathbf{x},t_n) &\approx \sum_{j=0}^{n}\int_\Gamma \omega_{n-j}\left(\Delta_t; G_{\mathbf{n},\star}(r)\right)\lambda^j(\mathbf{y})\,\mathrm{d}\Gamma_{\mathbf{y}}\end{aligned} \tag{48}$$

for $n=0,\dots,N$, where we have set $\psi^j(\mathbf{y}) := \psi(\mathbf{y},t_j)$ and $\lambda^j(\mathbf{y}) := \lambda(\mathbf{y},t_j)$.

In (48) the coefficients $\omega_n(\Delta_t; J_\star(r))$, $J_\star = G_\star, G_{\mathbf{n},\star}$ denote the quadrature weights associated to the convolution kernels $J_\star$, which are approximated by formula (A3).

The Laplace transforms $\widehat{J}_\star$, involved in (A3), can be computed by using some well known properties of the modified Bessel functions (see formulas 8.486(11,16,17) in [9]). In particular, we have that

$$\widehat{G}_\star(r,s) = \frac{1}{2\pi} K_0\left(\frac{rs}{v_\star}\right), \tag{49}$$

$$\widehat{G}_{\mathbf{n},\star}(r,s) = -\frac{s}{2\pi} K_1\left(\frac{rs}{v_\star}\right)\frac{\partial r}{\partial \mathbf{n}}, \tag{50}$$

where $K_0(z)$ and $K_1(z)$ are the second kind modified Bessel function of order 0 and 1, respectively.

For the computation of the solution $\mathbf{u}$ of Problem (1), according to Remark 3.1, we also need the Laplace transforms of the derivatives of $G_\star$ and $G_{\mathbf{n},\star}$ with respect to the variables $x_i, i = 1, 2$. These are given by (see [9] and [8])

$$\widehat{\frac{\partial G_\star}{\partial x_i}}(r,s) = -\frac{s}{2\pi} K_1\left(\frac{rs}{v_\star}\right)\frac{\partial r}{\partial x_i} \tag{51}$$

$$\widehat{\frac{\partial^2 G_\star}{\partial x_i \partial \mathbf{n}}}(r,s) = \frac{s^2}{2\pi v_\star^2}\left[\left(K_0\left(\frac{rs}{v_\star}\right) + \frac{v_\star}{rs} K_1\left(\frac{rs}{v_\star}\right)\right)\frac{\partial r}{\partial x_i}\frac{\partial r}{\partial \mathbf{n}} - \frac{v_\star}{s} K_1\left(\frac{rs}{v_\star}\right)\frac{\partial^2 r}{\partial x_i \partial \mathbf{n}}\right]. \tag{52}$$

Remark 3.2 *Taking into account the behaviours of $K_0(z)$ and $K_1(z)$, as $z \to 0$ (see [1]), straightforward calculation shows that the above two kernels have a singularity at $r = 0$ of the type r^{-1} the first, and of the type r^{-2} the second.*

To summarize, the temporal discretization of the TDBIE system is obtained by inserting in (42) the Lubich convolution quadrature formulas (48):

$$\begin{cases} \dfrac{1}{2}\varphi_P^n(\mathbf{x}) + \displaystyle\sum_{j=0}^{n}\int_\Gamma \omega_{n-j}\left(\Delta_t; G_{\mathbf{n},P}(r)\right)\varphi_P^j(\mathbf{y})\mathrm{d}\Gamma_\mathbf{y} - \sum_{j=0}^{n}\int_\Gamma \omega_{n-j}\left(\Delta_t; G_P(r)\right)\partial_{\boldsymbol{\tau}}\varphi_S^j(\mathbf{y})\mathrm{d}\Gamma_\mathbf{y} \\ \qquad = \displaystyle\sum_{j=0}^{n}\int_\Gamma \omega_{n-j}\left(\Delta_t; G_P(r)\right) g_\mathbf{n}^j(\mathbf{y})\mathrm{d}\Gamma_\mathbf{y} + I_{\varphi_{P,0}}(\mathbf{x},t_n) + I_{\bar{\varphi}_{P,0}}(\mathbf{x},t_n) + I_{\mathrm{f}_P}(\mathbf{x},t_n) \\ \dfrac{1}{2}\varphi_S^n(\mathbf{x}) + \displaystyle\sum_{j=0}^{n}\int_\Gamma \omega_{n-j}\left(\Delta_t; G_{\mathbf{n},S}(r)\right)\varphi_S^j(\mathbf{y})\mathrm{d}\Gamma_\mathbf{y} + \sum_{j=0}^{n}\int_\Gamma \omega_{n-j}\left(\Delta_t; G_S(r)\right)\partial_{\boldsymbol{\tau}}\varphi_P^j(\mathbf{y})\mathrm{d}\Gamma_\mathbf{y} \\ \qquad = \displaystyle\sum_{j=0}^{n}\int_\Gamma \omega_{n-j}\left(\Delta_t; G_S(r)\right) g_{\boldsymbol{\tau}}^j(\mathbf{y})\mathrm{d}\Gamma_\mathbf{y} + I_{\varphi_{S,0}}(\mathbf{x},t_n) + I_{\bar{\varphi}_{S,0}}(\mathbf{x},t_n) + I_{\mathrm{f}_S}(\mathbf{x},t_n), \end{cases} \tag{53}$$

for all $n = 0, \ldots, N$.

In what follows, after having introduced the parametric representation (12) of Γ, for the computation of the derivatives $\partial_{\boldsymbol{\tau}}\varphi_\star^j$, it is convenient to consider the curvilinear abscissa γ on Γ which, we recall, is defined by

$$\gamma = \gamma(\vartheta) = \int_0^\vartheta \|\boldsymbol{\eta}'(s)\|\,\mathrm{d}s, \qquad \vartheta \in [0,1]. \tag{54}$$

Since for any smooth enough scalar function ϕ it holds $\partial_{\boldsymbol{\tau}}\phi(\mathbf{y}) = \partial_\gamma \phi(\boldsymbol{\eta}(\vartheta))$, we will compute the derivatives $\partial_\gamma \varphi_\star^j(\boldsymbol{\eta}(\vartheta))$ in place of $\partial_{\boldsymbol{\tau}}\varphi_\star^j(\mathbf{y})$.

3.1.2 Space discretization

Let Γ be described by (12). We approximate the unknowns $\varphi_\star^j(\mathbf{x})$ and $\partial_\gamma\varphi_\star^j(\mathbf{x})$ for $\mathbf{x}\in\Gamma$ by

$$\varphi_\star^j(\boldsymbol{\eta}(\vartheta)) \approx \sum_{k=1}^{M+1} \varphi_{\star,k}^j N_k(\vartheta), \quad \partial_\gamma\varphi_\star^j(\boldsymbol{\eta}(\vartheta)) \approx \sum_{k=1}^{M+1} \varphi_{\star,k}^j \partial_\gamma N_k(\vartheta) \tag{55}$$

where, we recall, N_k's are the standard continuous piecewise linear basis functions associated with the partition $\{\vartheta_k\}_{k=1}^{M+1}$ of the parametrization interval $[0,1]$.

Remark 3.3 *If Γ is a circumference of radius R, as in our numerical tests, we have*

$$\mathbf{x} = \boldsymbol{\eta}(\vartheta) = R(\cos 2\pi\vartheta, \sin 2\pi\vartheta), \qquad \vartheta\in[0,1].$$

In this case $\gamma = 2\pi R\vartheta$ and for the derivatives in (55) we have

$$\partial_\gamma N_k(\vartheta) = \frac{\mathrm{d}N_k(\vartheta)}{\mathrm{d}\vartheta}\frac{\mathrm{d}\vartheta}{\mathrm{d}\gamma} = \begin{cases} 1/(2\pi R), & \text{if } \vartheta\in[\vartheta_{k-1},\vartheta_k],\ k>1 \\ -1/(2\pi R), & \text{if } \vartheta\in[\vartheta_k,\vartheta_{k+1}],\ k<M \\ 0, & \text{otherwise.} \end{cases}$$

Remark 3.4 *In the case where a global parametric representation of Γ is not given, a local one can be considered. To this aim, introducing a set of points $\{\mathbf{x}_k\}_{k=1}^{M+1}$ on Γ, we can define a local parametric representation of the arc $\widehat{\Gamma}_k\subset\Gamma$, joining the two mesh points $\mathbf{x}_k$, $\mathbf{x}_{k+1}$, by*

$$\mathbf{x} = \boldsymbol{\eta}_k(\vartheta) = (\eta_{1,k}(\vartheta), \eta_{2,k}(\vartheta)), \qquad \vartheta\in[0,1].$$

Then, we approximate the unknown functions by

$$\varphi_\star^j(\mathbf{x}) \approx \sum_{k=1}^{M+1} \varphi_{\star,k}^j b_k(\mathbf{x}), \tag{56}$$

where the b_k's are piecewise linear Lagrangian basis functions. In this case the curvilinear abscissa γ in (54) on each arc $\widehat{\Gamma}_k$ has its own representation

$$\gamma_k(\vartheta) = \int_0^\vartheta \|\boldsymbol{\eta}_k'(s)\|\,\mathrm{d}s, \qquad \vartheta\in[0,1]. \tag{57}$$

The corresponding derivative $\partial_\gamma b_k$ is then given by

$$\partial_\gamma b_k(\mathbf{x}) = \begin{cases} \dfrac{\mathrm{d}b_k(\boldsymbol{\eta}_{k-1}(\vartheta))}{\mathrm{d}\vartheta}\dfrac{\mathrm{d}\vartheta}{\mathrm{d}\gamma_{k-1}}, & \text{if } \mathbf{x}\in\widehat{\Gamma}_{k-1} \\ \dfrac{\mathrm{d}b_k(\boldsymbol{\eta}_k(\vartheta))}{\mathrm{d}\vartheta}\dfrac{\mathrm{d}\vartheta}{\mathrm{d}\gamma_k}, & \text{if } \mathbf{x}\in\widehat{\Gamma}_k \\ 0, & \text{otherwise.} \end{cases} \tag{58}$$

It is worthy to note that, for the approach that approximates simultaneously the boundary Γ and the unknowns $\varphi_\star^j$ by polygonal functions defined on the same uniform mesh, we can define

$$\mathbf{x} = \boldsymbol{\eta}_k(\vartheta) = (1-\vartheta)\mathbf{x}_k + \vartheta\mathbf{x}_{k+1}, \qquad \vartheta\in[0,1].$$

Since $\gamma_k = L_k\vartheta$, *where* $L_k = \|\mathbf{x}_{k+1} - \mathbf{x}_k\|$ *and the basis functions* b_k *are defined by*

$$b_k(\mathbf{x}) = \begin{cases} b_k(\boldsymbol{\eta}_{k-1}(\vartheta)) = \vartheta, & \text{if } \mathbf{x} \in \widehat{\Gamma}_{k-1} \\ b_k(\boldsymbol{\eta}_k(\vartheta)) = 1 - \vartheta, & \text{if } \mathbf{x} \in \widehat{\Gamma}_k \\ 0, & \text{otherwise,} \end{cases}$$

the derivatives in (58) *take the very simple form:*

$$\partial_\gamma b_k(\mathbf{x}) = \begin{cases} 1/L_{k-1}, & \text{if } \mathbf{x} \in \widehat{\Gamma}_{k-1} \\ -1/L_k, & \text{if } \mathbf{x} \in \widehat{\Gamma}_k \\ 0, & \text{otherwise.} \end{cases}$$

In order to apply a nodal collocation method, we approximate $g^j_{\mathbf{n}}$ and $g^j_{\boldsymbol{\tau}}$ by the interpolant piecewise linear function in terms of the basis functions N_k, we insert (55) into (53) and we collocate the latter at the collocation points ϑ_m, $m = 1, \ldots, M+1$.

By using (A4) in (53), we introduce the matrix notation:

$$(\mathbf{V}^n_\star)_{m,k} := \frac{1}{2\pi}\frac{\varrho^{-n}}{L}\sum_{l=0}^{L-1}\left(\int_0^1 K_0\left(\frac{r_m z}{v_\star}\right) N_k(\vartheta)\,\|\boldsymbol{\eta}'(\vartheta)\|\,\mathrm{d}\vartheta\right)\mathrm{e}^{-\frac{\imath n l 2\pi}{L}} \tag{59}$$

$$(\widetilde{\mathbf{V}}^n_\star)_{m,k} := \frac{1}{2\pi}\frac{\varrho^{-n}}{L}\sum_{l=0}^{L-1}\left(\int_0^1 K_0\left(\frac{r_m z}{v_\star}\right) \partial_\tau N_k(\vartheta)\,\|\boldsymbol{\eta}'(\vartheta)\|\,\mathrm{d}\vartheta\right)\mathrm{e}^{-\frac{\imath n l 2\pi}{L}} \tag{60}$$

$$(\mathbf{K}^n_\star)_{m,k} := -\frac{1}{2\pi}\frac{\varrho^{-n}}{L}\sum_{l=0}^{L-1}\left(\int_0^1 sK_1\left(\frac{r_m z}{v_\star}\right) \frac{\partial r}{\partial \mathbf{n}} N_k(\vartheta)\,\|\boldsymbol{\eta}'(\vartheta)\|\,\mathrm{d}\vartheta\right)\mathrm{e}^{-\frac{\imath n l 2\pi}{L}} \tag{61}$$

where $z := \gamma(\varrho \mathrm{e}^{\imath l 2\pi/L})/\Delta_t$ and $r_m = \|\boldsymbol{\eta}(\vartheta_m) - \boldsymbol{\eta}(\vartheta)\|$.

Finally, setting $\boldsymbol{g}^j_{\mathbf{n}} := \left[g^j_{\mathbf{n}}(\boldsymbol{\eta}(\vartheta_1)), \ldots, g^j_{\mathbf{n}}(\boldsymbol{\eta}(\vartheta_{M+1}))\right]^T$ and $\boldsymbol{g}^j_{\boldsymbol{\tau}} := \left[g^j_{\boldsymbol{\tau}}(\boldsymbol{\eta}(\vartheta_1)), \ldots, g^j_{\boldsymbol{\tau}}(\boldsymbol{\eta}(\vartheta_{M+1}))\right]^T$, we get the following system

$$\begin{cases} \dfrac{1}{2}\boldsymbol{\varphi}^n_P + \displaystyle\sum_{j=0}^{n}\mathbf{K}^{n-j}_P\boldsymbol{\varphi}^j_P - \sum_{j=0}^{n}\widetilde{\mathbf{V}}^{n-j}_P\boldsymbol{\varphi}^j_S = \sum_{j=0}^{n}\mathbf{V}^{n-j}_P\,\boldsymbol{g}^j_{\mathbf{n}} + \mathbf{I}^n_{\varphi_{P,0}} + \mathbf{I}^n_{\bar{\varphi}_{P,0}} + \mathbf{I}^n_{\mathrm{f}_P} =: \mathbf{d}^n_P \\ \dfrac{1}{2}\boldsymbol{\varphi}^n_S + \displaystyle\sum_{j=0}^{n}\mathbf{K}^{n-j}_S\boldsymbol{\varphi}^j_S + \sum_{j=0}^{n}\widetilde{\mathbf{V}}^{n-j}_S\boldsymbol{\varphi}^j_P = \sum_{j=0}^{n}\mathbf{V}^{n-j}_S\,\boldsymbol{g}^j_{\boldsymbol{\tau}} + \mathbf{I}^n_{\varphi_{S,0}} + \mathbf{I}^n_{\bar{\varphi}_{S,0}} + \mathbf{I}^n_{\mathrm{f}_S} =: \mathbf{d}^n_S \end{cases} \tag{62}$$

in the unknowns $\boldsymbol{\varphi}^n_\star = (\varphi^n_{\star,1}, \ldots, \varphi^n_{\star,M+1})^T$.

In matrix form the final linear system is

$$\begin{pmatrix} \dfrac{1}{2}\mathbf{I} + \mathbf{K}^0_P & -\widetilde{\mathbf{V}}^0_P \\ \widetilde{\mathbf{V}}^0_S & \dfrac{1}{2}\mathbf{I} + \mathbf{K}^0_S \end{pmatrix}\begin{pmatrix} \boldsymbol{\varphi}^n_P \\ \boldsymbol{\varphi}^n_S \end{pmatrix} = -\sum_{j=0}^{n-1}\begin{pmatrix} \mathbf{K}^{n-j}_P & -\widetilde{\mathbf{V}}^{n-j}_P \\ \mathbf{K}^{n-j}_S & \widetilde{\mathbf{V}}^{n-j}_S \end{pmatrix}\begin{pmatrix} \boldsymbol{\varphi}^j_P \\ \boldsymbol{\varphi}^j_S \end{pmatrix} + \begin{pmatrix} \mathbf{d}^n_P \\ \mathbf{d}^n_S \end{pmatrix}. \tag{63}$$

Note that when the boundary Γ is a circle and the chosen mesh points $\{\mathbf{x}_k\}$ are equidistant, all matrix blocks of the above system have the Toeplitz form. This means that only the first row of each block needs to be determined.

Finally, we remark that for the computation of the matrix entries (59)–(61), following the numerical procedure described in [7] and [8], we have applied a ν-point Gauss-Legendre quadrature formula, after introducing the polynomial smoothing transformation when the kernel K_0 displays the log behaviour. Details concerning the computation of these entries and of the volume integrals defining the known terms $\mathbf{d}_\star^n$ in (63) are postponed to the next section.

In the next section we present some numerical test aiming at comparing the classical TDBIE formulation for Problem (1), described in Section 2, with the new approach we have described in Section 3. These highlight some advantages of the novel strategy with respect to the standard one: the expression of the Laplace transforms of the integral kernels are more regular and easy to handle; the efficient computation of the integrals, defining the matrix entries of the associated linear system, does not require any tailored quadrature (in the examples reported in the next section a 8-point Gauss-Legendre rule has been used); the Toeplitz structure of the matrices when the boundary Γ is a circle allows to speed up significantly the computation and to save memory space. All these features are certainly of interest in the case of a BEM-FEM approach where the chosen artificial boundary is a circle (see [6]).

4 Numerical results

Since by a simple change of variables we can always normalize the obstacle dimension and the S-wave propagation velocity, in the examples reported below the obstacle is a circle of radius 1 and, in the first two examples, $v_S = 1$, $v_P = \sqrt{3}$. Furthermore, since the elastodynamic equation (1) can be rewritten in the form

$$\frac{\partial^2 \mathbf{u}}{\partial t^2}(\mathbf{x},t) - (v_P^2 - v_S^2)\nabla(\operatorname{div}\mathbf{u})(\mathbf{x},t) - v_S^2\nabla^2\mathbf{u}(\mathbf{x},t) = \frac{1}{\rho}\mathbf{f}(\mathbf{x},t)$$

in the first two examples we do not choose specific values of λ and μ. We also remark that although the above mentioned change of variables modify the force $\mathbf{f}$ by introducing the factor $[R^2 v_S^2]^{-1}$, where R denotes the original obstacle radius, for simplicity we assume that this factor is included in the expression defining $\mathbf{f}$.

Example 1. In this preliminary test we compare the convergence behaviour of the two analyzed approaches. To this end, we consider Problem (1) defined on the exterior of the unit disc centered at the origin of the axes, with homogeneous initial data and null source $\mathbf{f}$. The Dirichlet datum is $\mathbf{g} = (\mathrm{g}_1, \mathrm{g}_2)$, where

$$\mathrm{g}_1(\mathbf{x},t) = t^3 \mathrm{e}^{-2t}\mathrm{e}^{-(x_1^2+2x_2^2)}, \qquad \mathrm{g}_2(\mathbf{x},t) = t^3\mathrm{e}^{-2t}\cos(x_1), \qquad \mathbf{x}\in\Gamma,\ t\in[0,T],$$

with $T = 1$. In Table 1 we report the maximum in time of the L^2 errors

$$\mathrm{E}_{L^2,f} = \max_{t\in[0,T]} \|f^{\mathrm{ex}}(\cdot,t) - f(\cdot,t)\|_{L^2(\Gamma)} \approx \max_{n=0,\ldots,N} \sqrt{\Delta_\vartheta \sum_{k=1}^{M} \Big(f^{\mathrm{ex}}(\boldsymbol{\eta}(\vartheta_k),t_n) - f(\boldsymbol{\eta}(\vartheta_k),t_n)\Big)^2} \tag{64}$$

being $f = \varphi_\star$, $\star = P, S$ for the new approach, and $f = t_\ell$, $\ell = 1, 2$ for the standard one. In (64), f^{ex} denotes the reference solutions obtained with $M^{\mathrm{ex}} = N^{\mathrm{ex}} = 2048$ for the new approach, and $M^{\mathrm{ex}} = N^{\mathrm{ex}} = 512$ for the standard one. The discretization parameter $\Delta_\vartheta = 2\pi/M$

denotes the step size of the uniform partitioning of the parametrization interval of the curve Γ into M subintervals. We remark that, being the obstacle a disc, for the new approach we could take advantage of the Toeplitz structure of the involved matrices at each time step and, consequently, we could perform an efficient matrix-vector product, without storing the whole matrices. This property allowed us to consider the quite fine discretization reference parameters $M^{\text{ex}} = N^{\text{ex}} = 2048$. On the contrary, in the standard elastodynamics approach, the matrices do not have the special Toeplitz structure and, therefore, we had to compute and store all their entries. For this reason the finer value of the discretization reference parameters we could consider is $M^{\text{ex}} = N^{\text{ex}} = 512$, since $M^{\text{ex}} = N^{\text{ex}} = 1024$ gave rise to an out of memory. Therefore, in the tables below, we denote by the symbol "$\times$" the errors that could not be computed.

As Table 1 shows, the approaches have a comparable order of accuracy and the corresponding EOC is quadratic, as expected. The numerical results corresponding to the standard approach have been obtained by using the tailored quadrature described in Section 2.1.3 by using a smoothing polynomial transformation of degree $q = 3$ (see [15] and [16]), $\varepsilon_m = 1.0e{-}02$ and $N_0 = 30$. These choices can not be considered optimal, but revealed to be effective for our purposes.

Table 1: Example 1. Maximum in time of the L^2 absolute errors and corresponding EOC.

$M = N$	$\mathrm{E}_{L^2,\varphi_P}$	EOC	$\mathrm{E}_{L^2,\varphi_S}$	EOC	E_{L^2,t_1}	EOC	E_{L^2,t_2}	EOC
8	$2.39e-02$		$1.71e-02$		$2.25e-02$		$4.94e-02$	
		1.4		1.2		1.6		1.8
16	$9.04e-03$		$7.59e-03$		$7.51e-03$		$1.39e-02$	
		1.9		1.9		2.0		1.8
32	$2.51e-03$		$2.10e-03$		$1.88e-03$		$4.09e-03$	
		2.0		2.0		2.1		1.8
64	$6.30e-04$		$5.27e-04$		$4.70e-04$		$1.20e-03$	
		2.0		2.0		2.3		2.2
128	$1.55e-04$		$1.29e-04$		$1.16e-04$		$3.10e-04$	
		2.1		2.1		2.3		2.3
256	$3.79e-05$		$3.15e-05$		$2.41e-05$		$6.47e-05$	
		2.3		2.3		$\times$		$\times$
512	$8.97e-06$		$7.46e-06$		$\times$		$\times$	
		2.3		2.3		$\times$		$\times$
1024	$1.79e-06$		$1.49e-06$		$\times$		$\times$	

In Table 2 we report the values of the approximations $\mathbf{u}^{\text{new}}(P) = (\mathrm{u}_1^{\text{new}}(P),\mathrm{u}_2^{\text{new}}(P))$ and $\mathbf{u}^{\text{std}}(P) = (\mathrm{u}_1^{\text{std}}(P),\mathrm{u}_2^{\text{std}}(P))$, given by the new and the standard approaches respectively, of the solution $\mathbf{u}$ of the original problem at the external point $P = (2, 0)$. We also report the EOC of the corresponding errors.

In Figures 1 and 2 we show the space (with respect to the parametrization interval) and time behaviour of the density functions φ_P, φ_S of the new approach and t_1 and t_2 of the standard one. In Figure 3 we show the good agreement of the solutions $\mathrm{u}_i^{\text{new}}(P,t)$ with $\mathrm{u}_i^{\text{std}}(P,t)$, $i = 1, 2$, at the exterior point $P = (2, 0)$ and by varying $t \in [0, T]$.

Finally, we remark that, from an intensive numerical testing, it results that both approaches are numerically stable for any choice of the discretization parameters, even for long times T. As an example, in Figures 4 and 5 we show the space-time behaviour of the density functions φ_P, φ_S of the new approach and t_1 and t_2 of the standard one, for $T = 10$. In Figure 6 we

Table 2: Example 1. Approximations $\mathbf{u}^{\text{new}}$and $\mathbf{u}^{\text{std}}$at P=(2,0) and $T = 1$.

$M = N$	$\mathrm{u}_1^{\text{new}}(P,\mathrm{T})$	EOC	$\mathrm{u}_2^{\text{new}}(P,\mathrm{T})$	EOC	$\mathrm{u}_1^{\text{std}}(P,\mathrm{T})$	EOC	$\mathrm{u}_2^{\text{std}}(P,\mathrm{T})$	EOC
8	$6.63586e-03$		$-9.91880e-04$		$7.60399e-03$		$-6.04807e-04$	
		1.1		1.1		0.5		1.5
16	$7.39561e-03$		$-1.20263e-03$		$7.75437e-03$		$-1.10216e-03$	
		1.9		1.3		2.1		1.5
32	$7.90670e-03$		$-1.30820e-03$		$8.01355e-03$		$-1.28358e-03$	
		2.0		1.6		2.1		1.8
64	$8.04662e-03$		$-1.35790e-03$		$8.07430e-03$		$-1.35186e-03$	
		2.0		1.8		2.3		2.1
128	$8.08192e-03$		$-1.37534e-03$		$8.08888e-03$		$-1.37384e-03$	
		2.1		1.9		2.3		2.1
256	$8.09070e-03$		$-1.38073e-03$		$8.09244e-03$		$-1.38036e-03$	
		2.3		2.2		×		×
512	$8.09288e-03$		$-1.38227e-03$		×		×	
		2.3		2.2		×		×
1024	$8.09343e-03$		$-1.38270e-03$		×		×	

Figure 1: Example 1. Behaviour of the density functions φ_P and φ_S for $T = 1$.

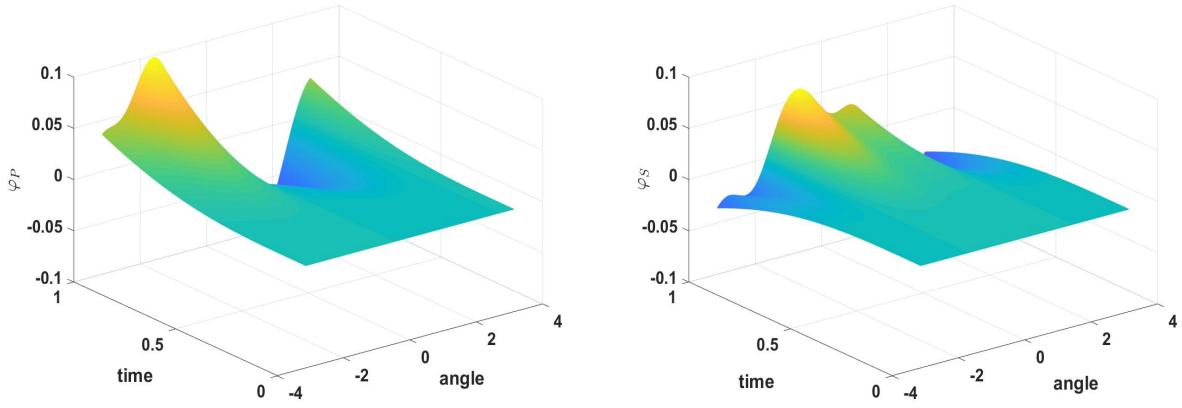

can see that the solutions $\mathrm{u}_i^{\text{new}}(P,t)$ and $\mathrm{u}_i^{\text{std}}(P,t)$, $i = 1,2$ given by the two approaches match also for long times.

Figure 2: Example 1. Behaviour of the density functions t_1 and t_2 for $T = 1$.

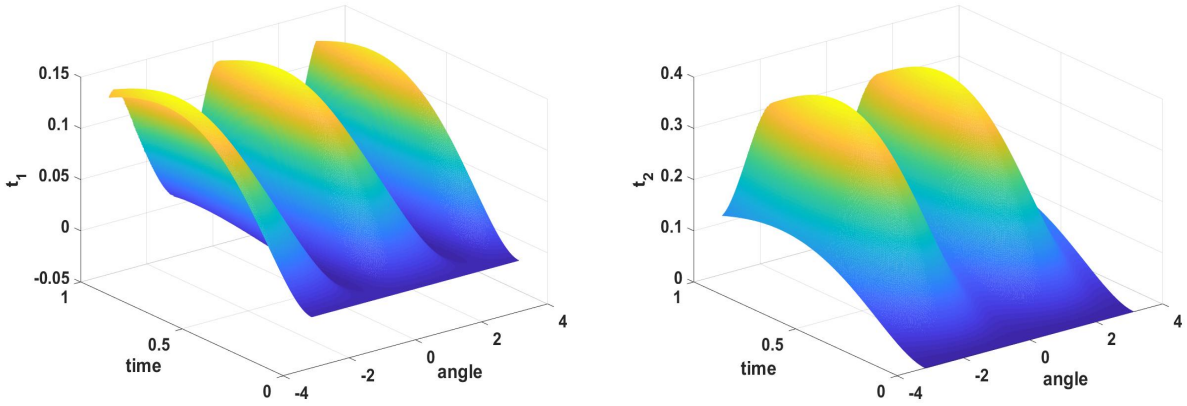

Figure 3: Example 1. Behaviour of the solutions $\mathbf{u}^{\mathrm{new}}(P,t)$ and $\mathbf{u}^{\mathrm{std}}(P,t)$ at $P = (2,0)$ for $t \in [0,1]$.

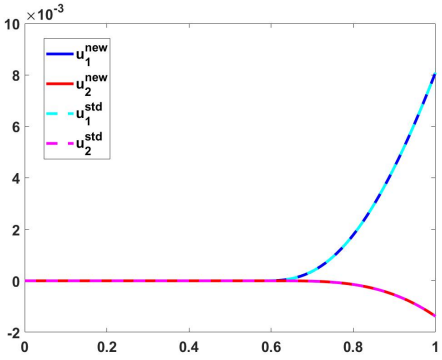

Figure 4: Example 1. Behaviour of the density functions φ_P and φ_S for $T = 10$.

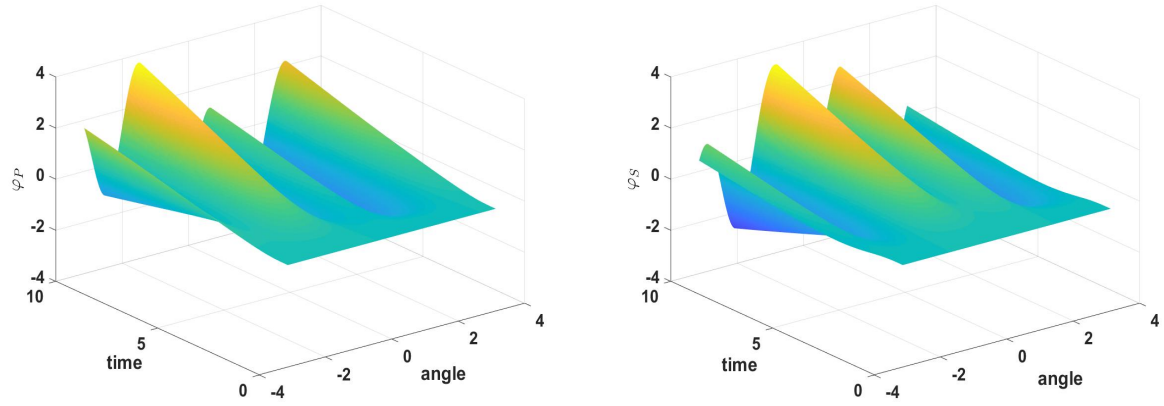

Figure 5: Example 1. Behaviour of the density functions t_1 and t_2 for $T = 10$.

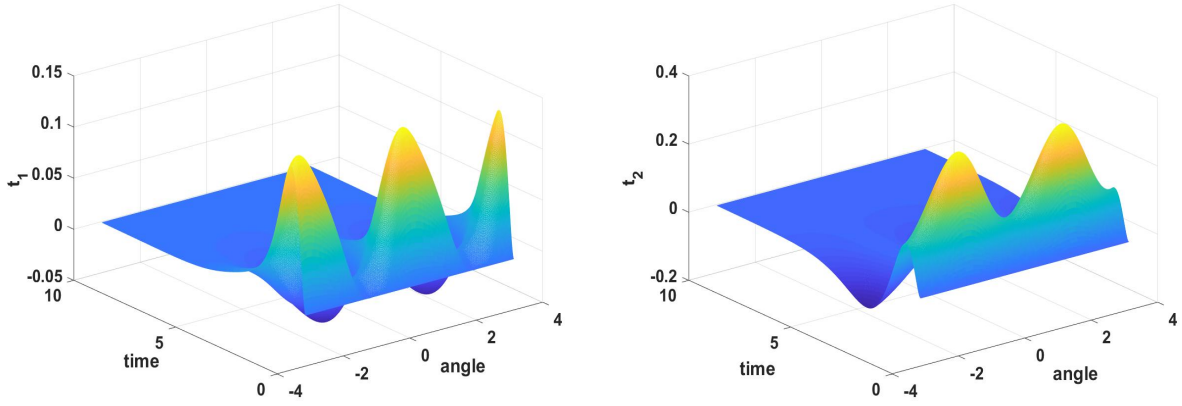

Figure 6: Example 1. Behaviour of the solutions $\mathbf{u}^{\mathrm{new}}(P,t)$ and $\mathbf{u}^{\mathrm{std}}(P,t)$ at $P = (2,0)$ for $t \in [0,10]$.

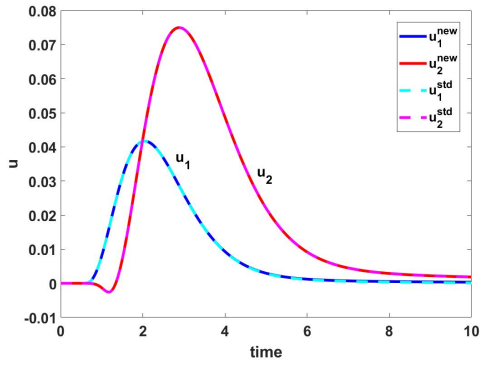

Example 2. We consider an elastic wave generated by a horizontally propagating incident wave

$$\mathbf{g}(\mathbf{x},t) = (g(x_1 - x_{1,0} + v_P t), 0)^T, \tag{65}$$

impinging on an obstacle represented by the unit disc centered in $(0,0)$. We consider $g(t) = e^{-20(t-t_0)^2}$, with $t_0 = 0.475$, $x_{1,0} = 2$ and the final time $T = 4$. The total field consists of the superposition of an incident and a scattered field $\mathbf{u}(\mathbf{x},t) = \mathbf{u}^{inc}(\mathbf{x},t) + \mathbf{u}^{scatt}(\mathbf{x},t)$, being $\mathbf{u}^{inc}(\mathbf{x},t) = -\mathbf{g}(\mathbf{x},t)$ for $\mathbf{x} \in \Omega^e$ and $\mathbf{u}^{scatt}$ the solution of Problem (1) with null $\mathbf{u}_0$ and $\mathbf{v}_0$ and Dirichlet datum $\mathbf{g}$ on Γ.

In Figure 7 we show the snapshots of the solution, obtained by the new numerical approach at the time instants $t = 0.5, 1, 1.25, 1.5, 1.75, 2, 2.25, 2.5, 2.75, 3$. The discretization parameters used to compute the approximate solution are $M = N = 128$. In the first and third column we represent the first component u_1 of the total field $\mathbf{u}$, in the second and fourth column the second one u_2. As expected, this latter appears once the solution u_1, generated by the datum g, bumps against the obstacle and is reflected back.

We remark that, for what concerns the standard approach, the reconstruction of the total external field revealed to be too expensive. For this reason we have compared the solutions $\mathbf{u}^{\mathrm{new}}(P,t)$ and $\mathbf{u}^{\mathrm{std}}(P,t)$ at some exterior points, observing a good agreement of the two approaches. As an example, in Figure 8 we show their behaviour at $P = (2,0)$ by varying $t \in [0,4]$.

In the last example we aim at simulating the seismic response of a linear elastic medium including a buried unlined tunnel to a wave generated by a source term $\mathbf{f}$. The contribution of this source is given by the corresponding volume integral in (3) for the standard approach, and by that in (44) for the novel one.

Example 3. The 2D tunnel section is the circle of radius $1\,m$ centered at $(0,0)$. We consider Problem (1) with the following physical material parameters: $\mu = 1.4e+09\,kg/(ms^2)$, $v_P = 1459.7\,m/s$, $v_S = 941.32\,m/s$ and $\rho = 1580\,kg/m^3$, which correspond to the clay elastic moduli (see Table at https://pangea. stanford.edu/courses/gp262/Notes/5.Elasticity.pdf).

By properly rescaling the velocities in such a way that $v_S = 1\,m/s$ ($v_P = 1.5507$), we observe the propagation in the temporal interval $[0,T]$, with $T = 20\,s$. The expression of the source is $\mathbf{f} = \nabla \mathrm{f}_P + \mathbf{curl}\,\mathrm{f}_S$, with $\mathrm{f}_P = 0$ and

$$\mathrm{f}_S = 10^{10} t^3 e^{-t} e^{-50[(x_1 - x_{1,0})^2 + (x_2 - x_{2,0})^2]}, \tag{66}$$

centered at $\mathbf{x}_0 = (x_{1,0}, x_{2,0}) = (3,0)$. We remark that, since f_S decays exponentially fast away from its center $\mathbf{x}_0$, it can be regarded as compactly supported from the computational point of view. Therefore, in the standard approach, the expression of the source volume integrals (3) takes the form:

$$I_{\mathrm{f}_i}(\mathbf{x},t) = \sum_{\ell=1}^{2} \int_0^t \int_{supp(\mathrm{f}_\ell)} U^*_{i\ell}(\mathbf{x} - \mathbf{y}, t - s)\mathrm{f}_\ell(\mathbf{y},s)\mathrm{d}\mathbf{y}\mathrm{d}s$$

with

$$\mathbf{f} = (\mathrm{f}_1, \mathrm{f}_2) = -10^{12} t^3 e^{-t} e^{-50[(x_1 - x_{1,0})^2 + (x_2 - x_{2,0})^2]} (x_2 - x_{2,0}, -(x_1 - x_{1,0}))^T.$$

For the new approach, the corresponding volume integrals (see (44)) are $I_{\mathrm{f}_P} = 0$ and

$$I_{\mathrm{f}_S}(\mathbf{x},t) = \frac{1}{\rho v_S^2} \int_0^t \int_{supp(\mathrm{f}_S)} G_S(\mathbf{x} - \mathbf{y}, t - s)\mathrm{f}_S(\mathbf{y},s)\mathrm{d}\mathbf{y}\mathrm{d}s.$$

Figure 7: Example 2. Snapshots of the solution $\mathbf{u}^{\text{new}}(P,t)$ at different instants.

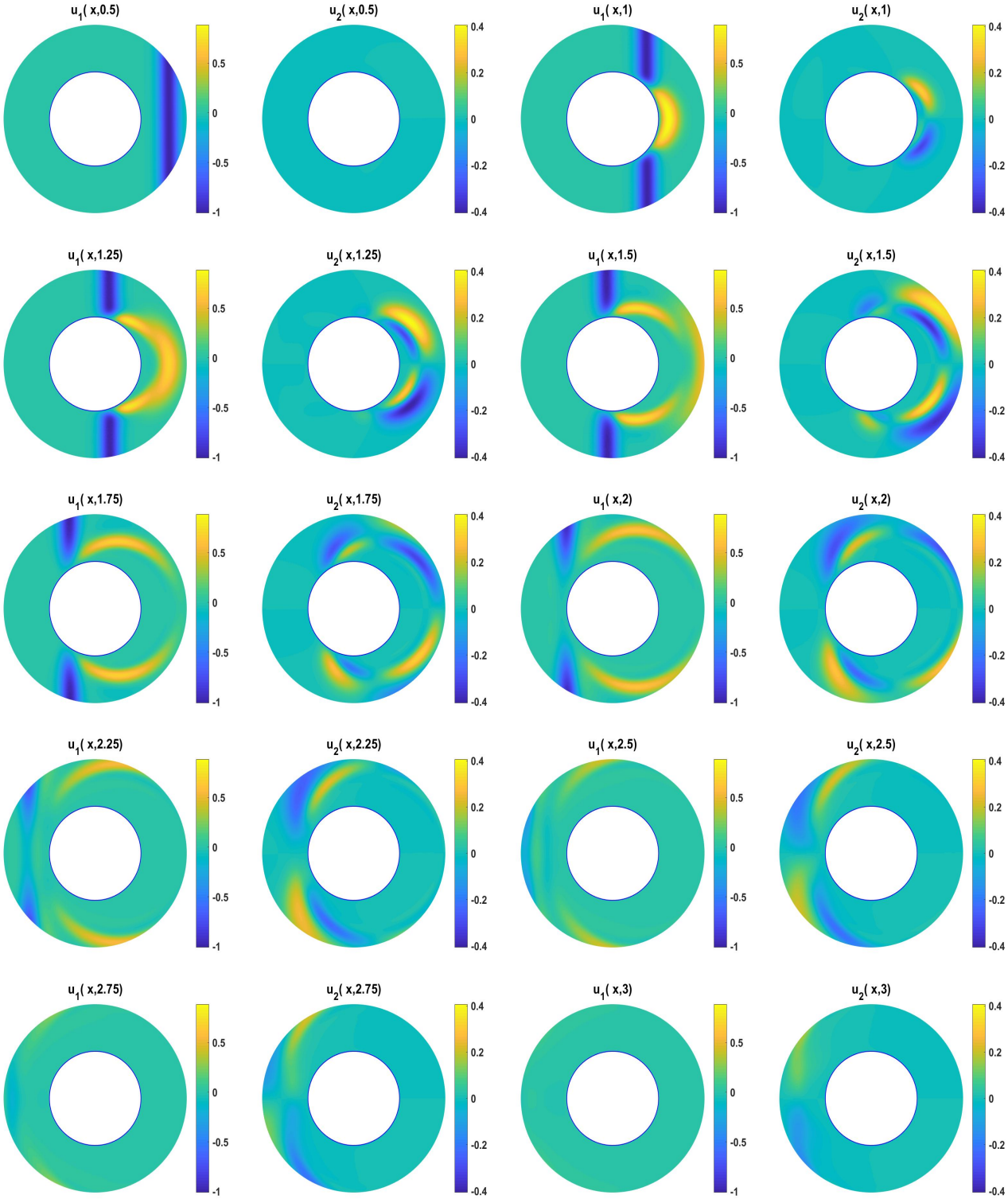

Figure 8: Example 2. Behaviour of the solutions $\mathbf{u}^{\text{new}}(P,t)$ and $\mathbf{u}^{\text{std}}(P,t)$ at $P=(2,0)$ for $t\in[0,4]$.

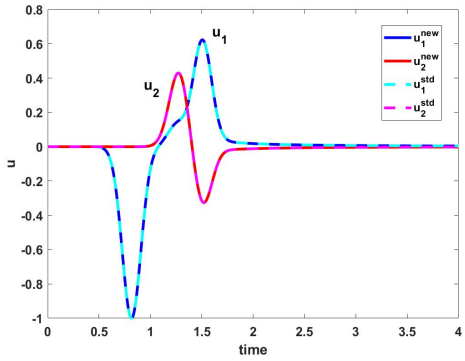

For the numerical computation of such integrals we have considered $supp(\mathrm{f}_\ell) = supp(\mathrm{f}_S) = \{\mathbf{x}\in\mathbb{R}^2 : \|\mathbf{x}-\mathbf{x}_0\|\le 1\}$, since at the boundary of such support f_S assumes values of order $1.0e-22$ and f_ℓ values of order $1.0e-20$. Then we have applied the 8×8-point Gauss-Legendre quadrature rule in space and a BDF2 Lubich convolution quadrature in time, based on the decomposition of the time interval $[0,T]$ into N subintervals.

Figure 9: Example 3. Behaviour of the density functions φ_P and φ_S for the local source (66), $t\in[0,20]$.

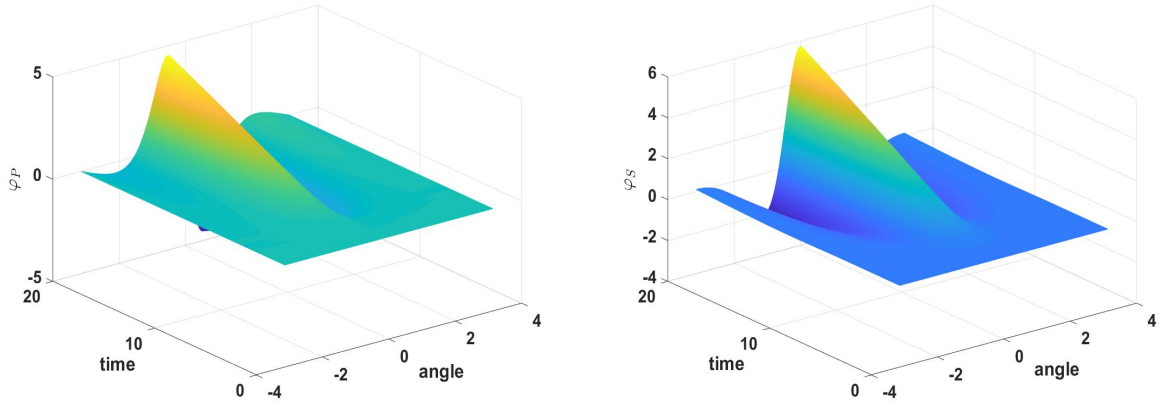

In Figures 9 and 10 we show the density functions of the two approaches. We remark that, for the standard method, the accurate computation of the integrals defining the matrix entries by the smoothing transformation and the series expansion of the Bessel functions, revealed to be crucial to obtain a reliable solution. Indeed, without the above tricks, spurious oscillations appear in the tractions t_1 and t_2, as Figure 11 shows. We remark that these oscillations do not disappear by increasing the number of the quadrature nodes, rather they get worse because the aforesaid apparent singularities do not cancel out numerically. In Figure 12 we show the good agreement of the solutions $\mathrm{u}_i^{\text{new}}(P,t)$ with $\mathrm{u}_i^{\text{std}}(P,t)$, $i=1,2$, at the exterior point $P=1.5(\cos(\pi/4),\sin(\pi/4))$ and by varying $t\in[0,20]$.

Figure 10: Example 3. Behaviour of the density functions t_1 and t_2 for the local source (66), $t \in [0, 20]$.

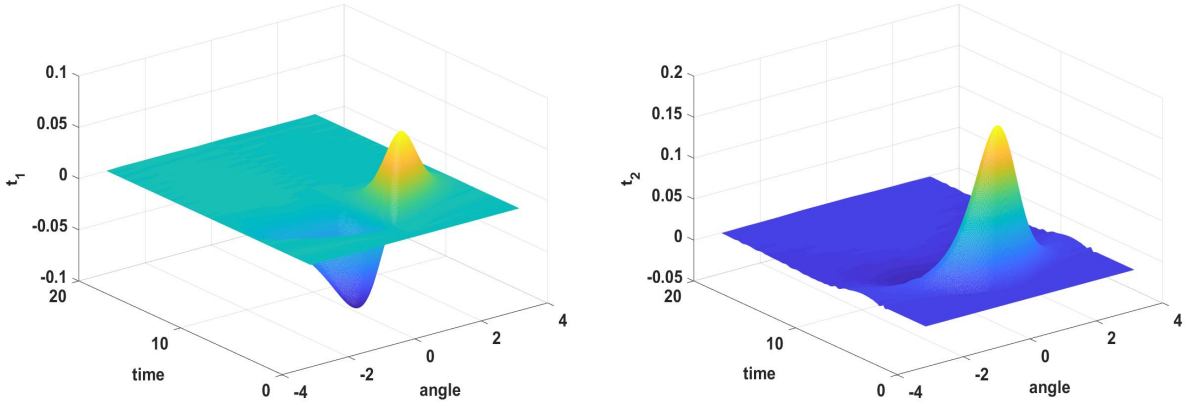

Finally, as last test, in the same setting of the previous case, we consider a wave generated by a point source, $\mathbf{f} = \nabla \mathrm{f}_P + \mathbf{curl}\, \mathrm{f}_S$, with $\mathrm{f}_S = 0$ and

$$\mathrm{f}_P = h(t)\delta(\mathbf{x} - \mathbf{x}_0), \qquad h(t) = 10^{10} t^3 e^{-2t} \sin(4t), \quad \mathbf{x}_0 = (10, 0). \tag{67}$$

For this choice, it is possible to apply only the new approach. In this case, the source volume integrals given by (44) become $I_{\mathrm{f}_S} = 0$ and

$$I_{\mathrm{f}_P}(\mathbf{x}, t) = \frac{1}{\rho v_P^2} \int_0^t G_P(\mathbf{x} - \mathbf{x}_0, t - s) \mathrm{f}_P(\mathbf{x}_0, s) \mathrm{d}s.$$

This latter has been efficiently computed by the Lubich quadrature rule, with the same number N of time steps used in the numerical approach of the associated TDBIE.

In Figure 13 we show the 3D behaviour of the density functions φ_P and φ_S obtained by the space and time discretization parameters $M = 2048$ and $N = 2048$, respectively. Finally, in Figure 14 we show the solution $\mathrm{u}_i^{\mathrm{new}}(P, t)$ with $\mathbf{u}^{\mathrm{new}}(P, t)$, at the exterior point $P = 1.5(\cos(\pi/4), \sin(\pi/4))$ and by varying $t \in [0, 20]$.

Figure 11: Example 3. Behaviour of the density functions t_1 and t_2 for the local source (66), $t \in [0, 20]$ with spurious oscillations given by a non accurate computation of the integrals.

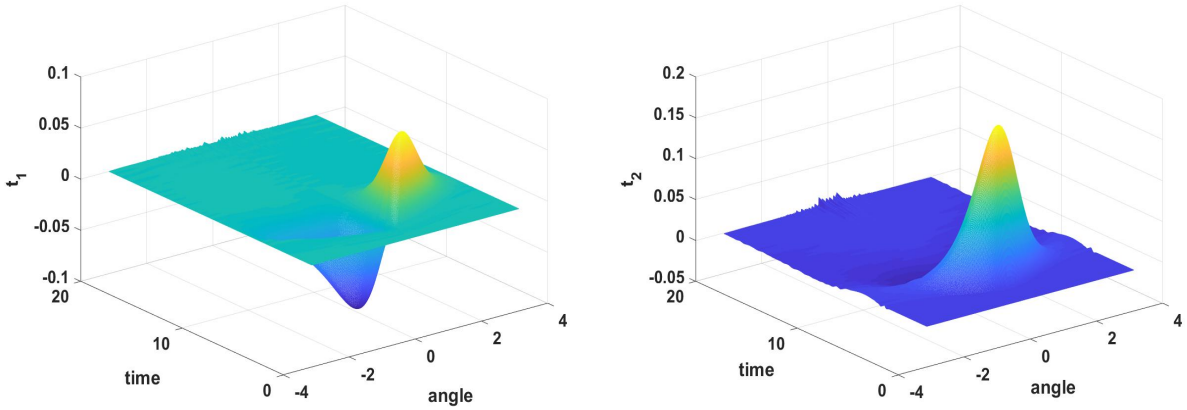

Figure 12: Example 3. Behaviour of the solutions $\mathbf{u}^{\text{new}}(P, t)$ and $\mathbf{u}^{\text{std}}(P, t)$ for the local source (66), $t \in [0, 20]$, $P = 1.5(\cos(\pi/4), \sin(\pi/4))$.

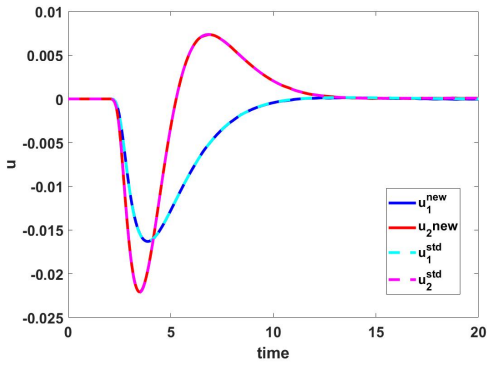

Figure 13: Example 3. Behaviour of the density functions φ_P and φ_S for the pointwise source (67), $t \in [0, 20]$.

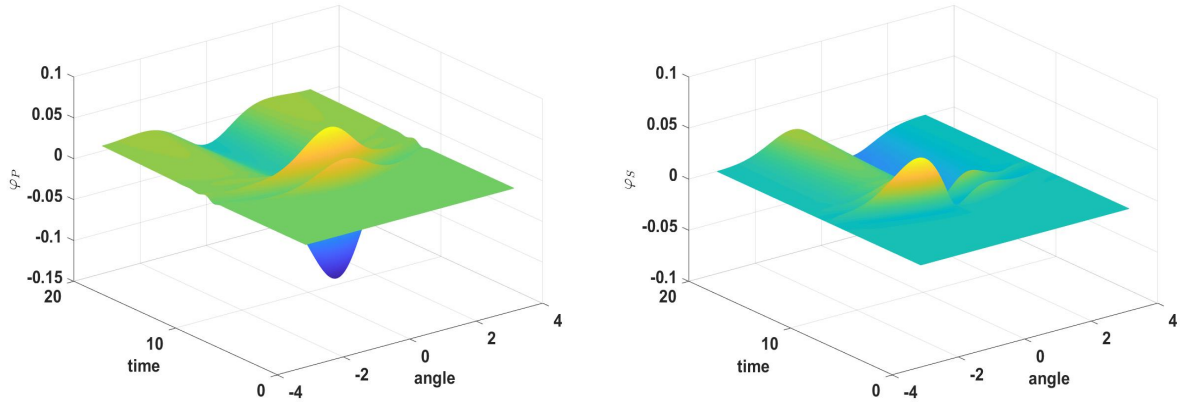

Figure 14: Example 3. Behaviour of the solution $\mathbf{u}^{\text{new}}(P, t)$ for the pointwise source (67), $t \in [0, 20]$, $P = 1.5(\cos(\pi/4), \sin(\pi/4))$.

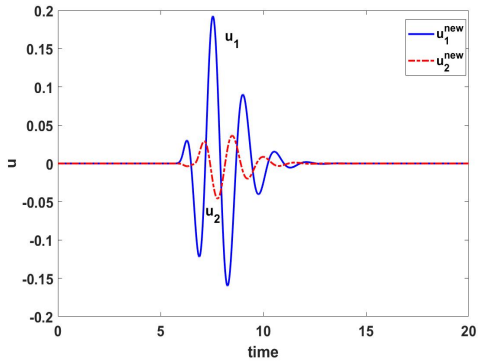

References

[1] M. Abramowitz and I. Stegun. *Handbook of Mathematical Functions*, volume 55. A.M.S. 55. National Bureau of Standards, Washington D.C., 1967.

[2] L. Banjai and M. Schanz. *Wave propagation problems treated with convolution quadrature and BEM.*, volume 63 of *Lecture Notes in Applied and Computational Mechanics*, pages 145–184. Fast Boundary Element Methods in Engineering and Industrial Applications, 2012.

[3] A. Burel, S. Impériale, and P. Joly. Solving the homogeneous isotropic linear elastodynamics equations using potentials and finite elements. The case of the rigid boundary condition. *Numer. Analys. Appl.*, 5(2):136–143, 2012.

[4] T.A Cruse and F.J. Rizzo. A direct formulation and numerical solution of the general transient elastodynamic problem. I. *J. Math. Anal. Appl.*, 22:244–259, 1968.

[5] A.C. Eringer and E.S. Suhubi. *Elastodynamics*, volume 2. Academic Press, New York, 1975.

[6] S. Falletta and G. Monegato. An exact non reflecting boundary condition for 2D time-dependent wave equation problems. *Wave Motion*, 51(1):168–192, 2014.

[7] S. Falletta, G. Monegato, and L. Scuderi. A space-time BIE methods for nonhomogeneous exterior wave equation problems. The Dirichlet case. *IMA J. Numer. Anal.*, 32(1):202–226, 2012.

[8] S. Falletta, G. Monegato, and L. Scuderi. A space-time BIE method for wave equation problems: the (two-dimensional) Neumann case. *IMA J. Numer. Anal.*, 34(1):390–434, 2014.

[9] I.S. Gradshteyn and I.M. Ryzhik. *Table of Integrals, Series, and Products*. Academic Press, New York, 2007.

[10] L. Kielhorn and M. Schanz. Convolution quadrature method-based symmetric Galerkin boundary element method for 3-D elastodynamics. *Int. J. Numer. Meth. Engng*, 76:1724–1746, 2008.

[11] C. Lubich. Convolution quadrature and discretized operational calculus. I. *Numer. Math.*, 52:129–145, 1988.

[12] J.A. Martinez, S. Impériale, P. Joly, and J. Rodriguez. Solving 2D linear isotropic elastodynamics by means of scalar potentials: a new challenge for finite elements. *HAL Id: hal-01803536, https://hal.inria.fr/hal-01803536*, 2018.

[13] T. Maruyama, T. Saitoh, T.Q. Bui, and S. Hirose. Transient elastic wave analysis of 3-D large-scale cavities by fast multipole BEM using implicit Runge-Kutta convolution quadrature. *Comput. Methods Appl. Mech. Engrg.*, 303:231–259, 2016.

[14] G. Monegato. Numerical evaluation of hypersingular integrals. *J. Comput. Appl. Math.*, 50:9–31, 1994.

[15] G. Monegato and L. Scuderi. High order methods for weakly singular integral equations with non smooth input functions. *Math. Comp.*, 67:1493–1515, 1998.

[16] G. Monegato and L. Scuderi. Numerical integration of functions with boundary singularities. *J. Comput. Appl. Math.*, 112:201–214, 1999.

[17] C.A.R. Vera-Tudela and J.C.F. Telles. 2D elastodynamic with boundary element method and the operational quadrature method. *Proceeding of COBEM 2005*, 18th International Congress of Mechanical Engineering, November 6–11 2005.

[18] C.C. Wang, H.C Wang, and G.S. Liou. Quadratic time domain BEM formulation for 2D elastodynamic transient analysis. *Int. J. Solids Structures*, 34(1):129–151, 1997.

Appendix

The BDF2-based Lubich quadrature formula

The convolution quadrature method proposed by Lubich [11] for the efficient computation of the convolution integral

$$\int_0^t k(t-s)\varphi(s)\mathrm{d}s, \qquad t \in [0,T]$$

is based on a uniform partitioning of the interval $[0,T]$ into N steps of equal length $\Delta_t = T/N$ and on the following formula

$$\int_0^{t_n} k(t_n-s)\varphi(s)\mathrm{d}s \approx \sum_{j=0}^{n} \omega_{n-j}(\Delta_t;K)\,\varphi(t_j), \qquad t_n = n\Delta_t,\ n=0,\ldots,N \tag{A1}$$

where, for each $j = 0,\ldots,N$,

$$\omega_j(\Delta_t;K) = \frac{1}{2\pi\imath}\int_{|z|=\varrho} K\left(\frac{\gamma(z)}{\Delta_t}\right) z^{-(j+1)}\mathrm{d}z, \tag{A2}$$

K being the Laplace transform of the convolution kernel k. In (A2) the function $\gamma(z) = 3/2 - 2z + 1/2z^2$ is the characteristic quotient of the BDF method of order 2 and ϱ is such that for $|z| \le \varrho$ the corresponding $\gamma(z)$ lies in the domain of analyticity of K.

By introducing the polar coordinate $z = \varrho \mathrm{e}^{\imath\vartheta}$ we have the following integral representation for the coefficients of formula (A2):

$$\omega_j(\Delta_t;K) = \frac{\varrho^{-j}}{2\pi}\int_0^{2\pi} K\left(\frac{\gamma(\varrho \mathrm{e}^{\imath\vartheta})}{\Delta_t}\right)\mathrm{e}^{-\imath j\varphi}\mathrm{d}\vartheta. \tag{A3}$$

This integral can be efficiently computed by using the trapezoidal rule, that is,

$$\omega_j(\Delta_t;K) \approx \frac{\varrho^{-j}}{L}\sum_{l=0}^{L-1} K\left(\frac{\gamma(\varrho \mathrm{e}^{\imath l\frac{2\pi}{L}})}{\Delta_t}\right)\mathrm{e}^{-\imath j l\frac{2\pi}{L}}, \qquad j=0,\ldots,N \tag{A4}$$

where the interval $[0,2\pi]$ has been partitioned into L subintervals of equal length. All the $\omega_j(\Delta_t;K)$ can be computed simultaneously by the FFT with $O(N\log N)$ flops. Assuming that K is computed with a relative accuracy bounded by ε, Lubich has shown that the choice $L = 2N$ and $\varrho^N = \sqrt{\varepsilon}$ leads to an approximation of ω_j with relative error of size $\sqrt{\varepsilon}$.